# High-quality eddy-covariance $CO_2$ budgets under cold climate conditions

Postprint version

**Fanny Kittler, Werner Eugster, Thomas Foken, Martin Heimann, Olaf Kolle, Mathias Göckede**

**Published in:** **Journal of Geophysical Research: Biogeosciences**

*This is the peer reviewed version of the following article:*

Kittler, F., W. Eugster, T. Foken, M. Heimann, O. Kolle, and M. Göckede (2017), High-quality eddy-covariance CO2 budgets under cold climate conditions, J. Geophys. Res. Biogeosci., 122, 2064–2084, doi:10.1002/2017JG003830.



**Contact:** **Fanny Kittler**

Department Biogeochemical Systems
Max Planck Institute for Biogeochemistry
Hans-Knoell-Str. 10
07745 Jena
Germany

e-mail: fkittler@bgc-jena.mpg.de

# High-quality eddy-covariance $CO_2$ budgets under cold climate conditions

Fanny Kittler, Werner Eugster, Thomas Foken, Martin Heimann, Olaf Kolle, Mathias Göckede

First published: 31 July 2017 https://doi.org/10.1002/2017JG003830

# Abstract

This study aimed at quantifying potential negative effects of instrument heating to improve eddy-covariance flux data quality in cold environments. Our overarching objective was to minimize heating-related bias in annual $CO_2$ budgets from an Arctic permafrost system. We used continuous eddy-covariance measurements covering three full years within an Arctic permafrost ecosystem with parallel sonic anemometers operation with activated heating and without heating as well as parallel operation of open- and closed-path gas analyzers, the latter serving as a reference. Our results demonstrate that the sonic anemometer heating has a direct effect on temperature measurements while the turbulent wind field is not affected. As a consequence, fluxes of sensible heat are increased by an average 5 W $m^{-2}$ with activated heating, while no direct effect on other scalar fluxes was observed. However, the biased measurements in sensible heat fluxes can have an indirect effect on the $CO_2$ fluxes in case they are used as input for a density-flux WPL correction of an open-path gas analyzer. Evaluating the self-heating effect of the open-path gas analyzer by comparing $CO_2$ flux measurements between open- and closed-path gas analyzers, we found systematically higher $CO_2$ uptake recorded with the open-path sensor, leading to a cumulative annual offset of 96 gC $m^{-2}$, which was not only the result of the cold winter season but also due to substantial self-heating effects during summer. With an inclined sensor mounting, only a fraction of the self-heating correction for vertically mounted instruments is required.

# 1 Introduction

Vast permafrost carbon pools threatened by amplified climate change effects make the Arctic a key region in the context of global climate change. Still, to date, only very limited information is available regarding cold season carbon cycle processes in Arctic permafrost ecosystems, mostly caused by highly challenging logistics and harsh environmental conditions. With the option to record continuous flux time series that are representative at the ecosystem scale [*Aubinet et al*., 2012], the network of eddy-covariance (EC) sites has grown considerably over the past decades, including coverage of complex terrain that is difficult to access with other monitoring techniques [*Eugster and Merbold*, 2015; *Foken*, 2017; *Monson and Baldocchi*, 2014; *Wyngaard*, 2010]. For Arctic environments, however, data coverage is still comparatively sparse [*Oechel et al*., 2014], largely linked to the challenges with respect to installation and selection of suitable instrumentation, power supply, and maintenance capacity. In addition, Arctic flux measurements may be negatively affected by heating effects of the instrumentation, particularly during Arctic winter conditions [*Goodrich et al*., 2016], causing, e.g., systematic biases in observed annual carbon budgets. Here we investigate these heating effects at a site in northeastern Siberia and develop suggestions how to minimize such biases.

The limitations of Arctic EC data coverage become particularly aggravated when it comes to flux observations beyond the growing season, since observations over the long winter season are still extremely rare. Consequently, in the past annual balances of Arctic EC fluxes were often estimated with crude approximations regarding wintertime fluxes; i.e., zero exchange from frozen soils was assumed. This approach has been shown to lead to systematic biases of the annual net $CO_2$ budgets in Arctic regions [*Euskirchen et al*., 2012; *Lüers et al*., 2014; *Marushchak et al*., 2013; *Oechel et al*., 2014; *Zimov et al*., 1996]. Nonzero wintertime $CO_2$ fluxes can, e.g., be linked to plant and microbial respiration of cold-tolerant species [*Bate and Smith*, 1983; *Coyne and Kelley*, 1974; *Kappen*, 1993; *Kelley et al*., 1968; *Panikov et al*., 2006], $CO_2$ loss during freeze-thaw dynamics [*Grogan et al*., 2004; *Pries et al*., 2013], free soil water creating warm microenvironments in frozen soils [*Zimov et al*., 1993], and unfrozen patches during the refreezing in the fall [*Mastepanov et al*., 2008; *Zona et al*., 2016]. Consequently, the continuous coverage of cold season $CO_2$ fluxes is critically important to assess the role of Arctic ecosystems within the context of global climate change.

As part of an EC system to monitor the $CO_2$ exchange, depending on the site characteristics and research purpose, open-path (OP) or closed-path (CP) gas analyzers can be used. Both options feature different advantages and disadvantages in their application [*Munger et al*., 2012]. Open-path configurations provide in situ measurements, while having a comparably low power and maintenance demand and are therefore widely used to determine $CO_2$ fluxes between the surface and the atmosphere [*Haslwanter et al*., 2009], especially in the Arctic. However, the operation of an open-path gas analyzer (LI-7500) may lead to systematic biases of $CO_2$ fluxes toward implausible uptake [*Amiro*, 2010; *Clement et al*., 2009; *Helbig et al*., 2016; *Oechel et al*., 2014; *Ono et al*., 2007] that can be linked to instrument heating. Heat is artificially generated by the instrument electronics housed below the optical path and results in higher temperatures within the optical path, generating an additional sensible heat flux inside the open optical measurement path. This effect has implications on the determined covariance, since this process is not accounted for by the traditional Webb-Pearman-Leuning (WPL) density-flux correction [*Webb et al*., 1980]. In an attempt to develop a direct instrumental solution for this problem, *Grelle and Burba* [2007] and *Massman and Frank* [2009] added fine-wire thermometers within the optical path of the LI-7500 to account for the influence of high-frequency temperature fluctuations. As a simplified alternative, a correction procedure to amend the performance of the instrument without the need for additional sensor installations was developed [*Burba et al*., 2006, 2008]. However, while the use of the self-heating correction has increased [*Reverter et al*., 2011], the application can vary depending on the instrumental setup [*Burba and Anderson*, 2010b]. The self-heating correction allows offsetting the flux biases induced by instrument self-heating [*Burba et al*., 2008; *Reverter et al*., 2011]. Alternatively, site-specific corrections can be determined using parallel CP measurements as a reference [*Järvi et al*., 2009]. If no parallel measurements are available, a generic scaling factor can be used [*Rogiers et al*., 2008]. Still, the self-heating correction for OP sensors is subject to large uncertainties, and it has been shown that its correct application needs to be customized for individual cases [*Bowling et al*., 2010; *Haslwanter et al*., 2009; *Wohlfahrt et al*., 2008]. Consequently, there is no general consensus on the application of the self-heating correction. Since the concept behind the correction assumes strongest heating effects under cold ambient air conditions [*Burba et al*., 2006, 2008], the correction is usually applied only for cold ecosystems.

Another important technical aspect for the operation of EC systems under cold Arctic conditions is the application of a heating device to avoid riming and/or icing at the transducers of the sonic anemometer. During periods with high air humidity in combination

with temperatures close to freezing, ice crystals can build up around the transducers of the sonic anemometer and disturb measurements [*Makkonen and Laakso*, 2005]. Heating systems to avoid ice buildup can be implemented as built-in versions by the manufacturer. Alternatively, customized versions can be installed using, e.g., heating tape or resistive heating wires wrapped around transducers [*Goodrich et al*., 2016; *Skelly et al*., 2002]. A suitable scheme to activate the heating device should be applied to ensure good instrument conditions and counteract icing events, but at the same time to minimize heating periods to avoid biasing the measurements. Increased sensible heat fluxes [*Skelly et al*., 2002] and resulting overestimations in carbon dioxide and latent heat fluxes [*Goodrich et al*., 2016] have been linked to active instrument heating. This calls for heating schemes that are based on meteorological conditions, triggering an activation, e.g., at high humidity and temperatures around freezing, instead of a continuous heating regardless of prevailing environmental conditions.

In summary there are several issues related to quantifying the turbulent $CO_2$ fluxes between the surface and the atmosphere and the estimation of reliable winter budgets in Arctic ecosystems. So far, no general recommendation to minimize associated data gaps, and particularly to avoid biases related to instrument heating, was developed. In this study we assess the quantitative effect of different instrument heating options: (1) the self-heating of the OP gas analyzer and (2) the heating of the sonic anemometer that was activated based on meteorological conditions. Measured scalars from both instruments, the vertical wind component from the sonic anemometer, and the $CO_2$ concentration from the OP system are essential to determine the turbulent $CO_2$ flux. Our findings build on continuous EC measurements from a field site near Chersky in northeastern Siberia covering three complete winter seasons. This data set covers parallel operation of heated and unheated sonic anemometers as well as parallel operation of OP and CP gas analyzer systems. This setup allows for a comprehensive assessment of the effect of different instrument heating options on continuous EC $CO_2$ flux measurements during Arctic winter and will be used to derive recommendations on how to minimize the bias in cases where only OP measurements are available. Therefore, both heating effects are analyzed separately and the effect of each heating system on the determined $CO_2$ exchange fluxes is evaluated. Different formulations on the self-heating effect (1) are introduced in section 2.3, corresponding results are presented in section 3.1, and these results are discussed in section 4.1. For analysis of an active sonic anemometer heating effect (2) the heating scheme is presented in section 2.4; results are described in section 3.2 and discussed in section 4.2.

# 2 Material and Methods

## 2.1 Instrumentation Setup

Measurements were carried out at a field site (68.75°N, 161.33°E) close to the city of Chersky in the northeastern part of Siberia, Russia. The study site was characterized as moist tussock tundra with a mean elevation of 6 m above sea level and an average snow depth of 0.6 to 1 m during winter. Two towers with an identical instrumentation were installed within a distance of about 600 m to monitor exchange fluxes between the surface and atmosphere. One tower is placed within a circular drainage ditch system, and the second tower reflects undisturbed conditions. While the analysis on the drainage disturbance focuses on the summer season, uniform conditions at both towers with frozen soil and a closed snow cover are assumed in the winter.

The EC instrumentation was mounted on top of each tower at a height of 4.9 m and 5.1 m for towers 1 and 2, respectively, including a heated sonic anemometer (uSonic-3 Scientific, former USA-1, METEK GmbH, Elmshorn, Germany; with integrated 55 W heating) and two types of gas analyzers (GA). The open-path GA (inclined by 15° toward ESE, LI-7500, LI-COR Biosciences Inc., NE, USA) was installed in summer 2013, while the closed-path GA (FGGA, Los Gatos Research Inc., CA, USA.) was added in spring 2014. The CP systems consist of an inlet placed next to the sonic anemometer (vertical sensor separation: 0.30 m), a sampling line (heated and insulated Eaton Synflex® (former name decabon) with 6.2 mm inner diameter and a length of 16.0 m and 12.8 m for towers 1 and 2, respectively, and an external vacuum pump (KNF N940 membrane pump, flow rate of 13 L $min^{-1}$ at ambient pressure).

Data collection was running continuously at both towers since the installation midsummer 2013 until spring 2016. Both GAs were running in parallel on tower 1 from spring 2014 until spring 2016, while on tower 2 the OP sensor was operational from July 2013 to July 2014, while afterward only the CP measurements were continued. For tower 2 the data collection was stopped in November 2015 due to a malfunction of the CP GA. While growing season measurements were reported by *Kittler et al*. [2016], the focus of the this study is on winter season, here defined as the period from 1 November to 31 March.

Ancillary measurements of barometric pressure (Pressure Transmitter, 61302 V, R.M. Young Company, Traverse City, USA), four radiation components (CNR4, Kipp & Zonen, Delft, Netherlands), and air temperature ($T_a$) and relative humidity (rH) combined (KPK 1/6-ME-H38, Mela, Bondorf, Germany, ventilated hut) were collected from the top of the towers and stored on a data logger (CR3000, Campbell Sci. Inc., Logan, USA).

## 2.2 Data Processing

Meteorological data were collected at 10 s intervals and stored on the data logger (CR3000, Campbell Scientific) as 10 min averages. Data postprocessing for these data follows a quality control scheme described in detail by *Kittler et al*. [2016]. Remaining high-quality data were subsequently averaged to 30 min intervals.

For the EC systems, data were collected at 20 Hz with analogue output for the GAs. Data acquisition on site used the software package EDDYMEAS [*Kolle and Rebmann*, 2007] on a local computer at the field site. Flux processing was handled with the TK3 software tool [*Mauder and Foken*, 2015], which implemented all required processing steps and correction procedures. For both, OP and CP GAs, the 2-D rotation of the wind field, the cross-wind correction [*Liu et al*., 2001], and a correction for loss in the high-frequency range [*Moore*, 1986] was applied. For the CP GA the high-frequency raw data (as wet mole fraction) were converted to dry mixing ratios before processing. Since losses in the high-frequency range occur when gases are transferred to the closed-path analyzers through inlet tubes, the flow rate of 13 L $min^{-1}$ (ambient pressure) translated into a replacement of sample air in the measurement cell at a frequency of ~2–2.5 Hz for $CO_2$ and $H_2O$, respectively, which were used as cutoff frequencies for the spectral correction of the CP GA. The WPL density-flux correction [*Webb et al*., 1980] was applied for the OP data to account for density fluctuations within the open optical measurement path.

To ensure high data quality, the standard postprocessing quality control scheme based on tests for stationarity and well-developed turbulence [*Foken and Wichura*, 1996] was extended by

additional tests to detect implausible data points in the resulting flux time series. These tests covered a check for absolute limits for $CO_2$ flux data ($-15$ μmol $m^{-2}$ $s^{-1}$ < $CO_2$ flux < 5 μmol $m^{-2}$ $s^{-1}$), the OP GA status information (gain control maximum < 75), errors messages in the log file reported by the sonic anemometer, a comparison of the absolute concentrations of $CO_2$ for the two towers for specific wind directions, a test for $T_a$ ($T_a$ < −40°C, which is the lowest possible operating $T_a$ for the sonic anemometer) and a flag for activated sonic anemometer heating. Quality flags (QFs) were combined, and data with highest quality (QF 1–3 [*Foken et al*., 2005, 2012]) were used for the detailed analysis for the self-heating of the OP instrument and the sonic anemometer heating effect (Table 1). For long-term budgets, data covering QF 1–6 [*Foken et al*., 2005, 2012] were used to increase data coverage for reliable and robust gap filling procedure (Table 1). The gap filling was based on the marginal distribution sampling method [*Reichstein et al*., 2005], implemented through the R-package "REddyProc" (https://r-forge.r-project.org/projects/reddyproc). For more details on quality tests and gap filling implementation see *Kittler et al*. [2016]. Statistics on data availability from both towers during the three winter seasons, broken up into data quality categories, are given in Table 1.

**Table 1**. Quality Flag (QF) of EC $CO_2$ Fluxes as Percentage of Winter Season (November–April) Measurements From Both Sites According to Foken et al. [2005, 2012].

| Site | Winter season | QF 1–3 (%) | QF 1–6 (%) |
|---|---|---|---|
| Tower 1 | 2013/2014 | 23.2 | 47.2 |
| | 2014/2015 | 21.8 | 60.9 |
| | 2015/2016 | 19.2 | 55.1 |
| Tower 2 | 2013/2014 | 18.5 | 44.2 |
| | 2014/2015 | 21.9 | 55.6 |
| | 2015/2016 | – | – |

Figure 1 lists the time frames used for studying self-heating effects of the LI-7500 as well as the sonic anemometer heating schemes as described in the following Sections. All statistical analyses were performed with the R software [*R Core Team*, 2014]. The examinations of the wind speed and direction with resulting figures were created with the R-package "openair" [*Carslaw*, 2015]. Because measurement signals of both the open- and closed-path gas analyzers have approximately the same error [*Dunn*, 2004], i.e., no one device is free of errors, the orthogonal regression was applied with the R-package "lmodel2" [*Legendre*, 2014]. Orthogonal regression analysis was used to assess the agreement between OP and CP flux measurements, and Pearson's correlation coefficients ($r$) are given. Orthogonal regression (linear model II regression) is used in place of ordinary least-square regression because it takes experimental uncertainties in both OP and CP measurements into account and does not require the definition of an independent and a dependent variable.

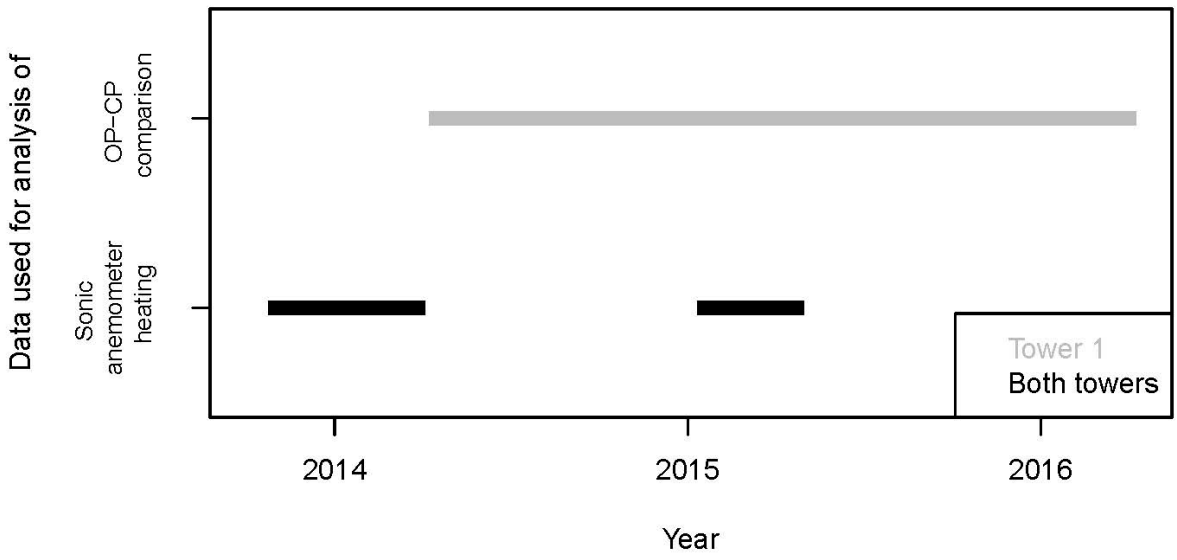


**Figure 1**. Time frames and used data for different analyses. Data coverage with QF 1–3.

### 2.3 Correction for Self-Heating of the Open-Path Sensor

To account for the self-heating of the OP analyzer, a correction was presented by *Burba et al*. [2008]. Their basic equation used to achieve final $CO_2$ fluxes ($F_c$), which includes an adjusted version of the original WPL flux-density formulation [*Webb et al*., 1980], corrects initial $CO_2$ fluxes ($F_0$) as

$$F_c = F_0 + \mu \frac{E}{\rho_d} \frac{\rho_c}{1 + \mu \frac{\rho_v}{\rho_d}} + \frac{S}{\rho c_p} \frac{\rho_c}{T_a}, \quad (1)$$

on the basis of equation (44) of *Webb et al*. [1980], while commonly equation (24) of *Webb et al*. [1980] is used [*Foken et al*., 2012; *Leuning*, 2004, 2007] with a numerical difference less than 1–2%. The WPL flux-density corrected latent heat flux is given as $E$ (kg m$^{-2}$ s$^{-1}$); $\rho_c$ (kg m$^{-3}$) as ambient $CO_2$ density; $\rho$ (kg m$^{-3}$) as total air mass density; $c_p$ (J kg$^{-1}$ K$^{-1}$) is the specific heat of air; $T_a$ (K) as the air temperature; $\mu$ is the molar mass ratio of dry air to water vapor given as 1.6077; $\rho_v$ (kg m$^{-3}$) and $\rho_d$ (kg m$^{-3}$) as partial densities of $H_2O$ and dry air, respectively; and $S$ (W m$^{-2}$) as the sensible heat flux. The resulting unit for the $CO_2$ flux is kg m$^{-2}$ s$^{-1}$. The sensible heat flux can be determined by different methods depending on the ancillary instrumentation [*Burba et al*., 2008]. Here we use "Method 4" from *Burba et al*. [2008] to estimate the self-heating correction as

$$S = \rho c_p \overline{w' T_a'} + S_{Burba}, \quad (2)$$

by combining elements from the WPL density-flux correction [*Webb et al*., 1980] as the first term on the right-hand side, while the second term represents the additional sensible heat flux caused by the self-heating of the instrument, here termed $S_{Burba}$. In *Burba et al*. [2008] the additional heat flux (here named $S_{Burba\_2008}$) was estimated based on the sensible heat flux from key instrument surfaces of the open-path instrument, namely, bottom, top, and spar of the sensor as

$$S_{Burba\_2008} = S^{bot} + S^{top} + 0.15\, S^{spar}. \quad (3)$$

Detailed equations to derive these separate heat fluxes that combine to the $S_{Burba\_2008}$ flux are listed in Table 2.

**Table 2.** Additional Formulations to Correct for the Self-Heating of an Open-Path LI7500 Gas Analyzer as Describe in *Burba et al*. [2008].

| Description | Formulation |
|---|---|
| S as sensible heat flux after Nobel [1983] with $r^{top}$ is 0.0225 m and $r^{spar}$ is 0.0025 m | $S^{bot} = k_{air}\frac{T_s^{bot} - T_a}{\delta^{bot}}$ <br> $S^{top} = k_{air}\frac{(r^{top} + \delta^{top})(T_s^{top} - T_{a)}}{r^{top}\delta^{top}}$ <br> $S^{spar} = k_{air}\frac{(T_s^{spar} - T_{a)}}{r^{spar} ln(\frac{r^{spar} + \delta^{top}}{r^{spar}})}$ |
| $\delta$ as average thickness of the boundary layer above the window with $l^{bot}$ is 0.065 m, $l^{top}$ is 0.045 m and $l^{spar}$ is 0.005 m | $\delta^{bot} = 0.004\sqrt{\frac{l^{bot}}{u}} + 0.004$ <br> $\delta^{top} = 0.0028\sqrt{\frac{l^{top}}{u}} + \frac{0.00025}{u} + 0.0045$ <br> $\delta^{spar} = 0.0058\sqrt{\frac{l^{spar}}{u}}$ |
| $T_s$ (K) as the instrument surface temperature with $T_o$ is 273.15 | $T_{s\_day}^{bot} = 0.944\,(T_a - T_0) + 2.57 + T_0$ <br> $T_{s\_night}^{bot} = 0.883(T_a - T_0) + 2.17 + T_0$ <br> $T_{s\_day}^{top} = 1.005\,(T_a - T_0) + 0.24 + T_0$ <br> $T_{s\_night}^{top} = 1.008\,(T_a - T_0) - 0.41 + T_0$ <br> $T_{s\_day}^{spar} = 1.01\,(T_a - T_0) + 0.36 + T_0$ <br> $T_{s\_night}^{spar} = 1.01\,(T_a - T_0) - 0.17 + T_0$ |

Since the traditional WPL flux-density correction [*Webb et al*., 1980] is commonly integrated in standardized processing software packages, the focus within this study has been placed on the self-heating term. Accordingly, to separate the self-heating term from the remaining steps, we combined equations 1 and 2 using already WPL density-flux [*Webb et al*., 1980] corrected $CO_2$ data ($F_{c\_WPL}$) as

$$F_c = F_{c\_WPL} + \xi\frac{S_{Burba}}{\rho c_p}\frac{\rho_c}{T_a}. \quad (4)$$

The scaling factor $\xi$ (−) introduced here is not part of the original equation and is explained in the next section. By using a combination of equations 4 and 3 this approach will hereafter be referred to as Burba_2008. A similar approach using $F_{c\_WPL}$ as input was proposed by *Burba et al*. [2006], here again slightly adjusted to achieve consistent units:

$$F_c = F_{c\_WPL} + \xi \frac{(T_s - T_a)\rho_c}{r_a T_a}\left(1 + \mu \frac{\rho_v}{\rho_d}\right), \quad (5)$$

$T_s$ (K) is the instrument surface temperature and $r_a$ (s m$^{-1}$) represents aerodynamic resistance. The aerodynamic resistance is determined directly from the friction velocity $u_*$ (m s$^{-1}$) and the horizontal wind speed $u$ (m s$^{-1}$) as $r_a = u/(u_*^2)$ according to the simplified bulk approach described in *Stull* [1988]. Note that we changed the originally used $q_c$ (μmol m$^{-3}$) for the ambient $CO_2$ density, which would have yielded $CO_2$ fluxes in μmol m$^{-2}$ s$^{-1}$, to $\rho_c$ (kg m$^{-3}$) as used in the preceding equations. This approach is referred to as Burba_2006.

The scaling factor $\xi$ represents the fraction of the self-induced heat flux relevant for the correction of an inclined LI-7500 sensor. Equation 5 was used by *Rogiers et al*. [2008] and further tested by *Järvi et al*. [2009], both pointing out that for inclined open-path analyzers only a small fraction of this additional heat flux actually influences the measurement path. Accordingly, $\xi$ can theoretically vary between 0 (no self-heating effect) and 1 (full self-heating effect needs to be applied, e.g., for a vertical sensor orientation). It was demonstrated by *Järvi et al*. [2009] that only a very small fraction of the full heat flux typically affects measurements that were taken with the recommended sensor inclination angle of 15°.

Putting the self-heating terms of the Burba_2008 and Burba_2006 approaches in relation (for details see equations (S1) to (S4) in the supporting information) by eliminating duplicate elements, neglecting the term $(1 + \mu\, \rho_v/\rho_d)$, since it only increases the heat flux term on the order of 2% and thus is not substantial, and application the formulation for $r_a$ follows

$$S_{Burba\_2006} = \frac{(T_s - T_a)\, u_*^2}{\mathrm{u}}\, \rho c_p. \quad (6)$$

Equation 6 as a reformulation for the additional sensible heat flux emitted by the open-path analyzer with the Burba_2006 approach reveals systematic differences between the approaches. In both cases, a temperature difference between air ($T_a$) and instrument surface ($T_s$) is the driving force of the heat flux. The simple Burba_2006 approach uses a bulk surface temperature and parameterized atmospheric resistance to derive heat fluxes. However, in the Burba_2008 approach surface temperatures are estimated for individual parts of the sensor and converted to individual heat fluxes using formulations proposed by *Nobel* [1983], and only afterward combined to a single instrument heat flux.

The instrument surface temperature is a crucial component of the self-heating correction that can be determined directly with additional measurements or can be estimated from $T_a$ based on various empirical parameterizations (in (K) with $T_o$ as absolute zero is 273.15). Due to radiative heating over the day and radiative cooling during the night affecting measurements differently with increased effects under nonvertical OP sensor configurations [*Burba et al*., 2008], some $T_s$ parameterizations differ between daytime and nighttime. Nighttime conditions were defined by incoming shortwave radiation <20 W m$^{-2}$. Consequently, Arctic winter with nearly no solar radiation is mostly represented by nighttime conditions, while during summer (June/July) ~70% of each day is characterized as daytime. While for equation 4 a set of surface temperature parameterizations for the different instrument parts are given (see Table 2), there is a bulk of parameterizations that can be used in combination with equation 5. Based on a polynomial fit from a field experiment:

$$T_s = 0.0025\,(T_a - T_0)^2 + 0.9\,(T_a - T_0) + 2.07 + T_0, \quad (7)$$

Equation 7 was found to best reproduce the observed heating effects and increased thermal exchange [Burba et al., 2006]. This equation was determined for the bottom part of the open path sensor, dominating under an inclined sensor mounting and is specified for a temperature range from −25°C to 20°C [Burba et al., 2006]. For a forest site, Järvi et al. [2009] developed separate fits for daytime and nighttime conditions in the temperature range of −12 to 28°C

$$T_{s\_day} = 0.93\ (T_a - T_0) + 3.17 + T_0 \text{ and } T_{s\_night} = 1.05\ (T_a - T_0) + 1.52 + T_0. \quad (8)$$

Under the assumption that the true flux was represented by the CP data, $\xi$ in equations 4 and 5 were optimized using a nonlinear least squares method to achieve optimum agreement between corrected OP and reference CP fluxes. For the optimization, the starting value for $\xi$ was set to 0.05, as suggested by other studies [*Järvi et al*., 2009; *Rogiers et al*., 2008]. The $\xi$ fraction was optimized separately for both the Burba_2008 and Burba_2006 approaches and also separately for the Burba_2006 approach with both $T_s$ parameterizations.

Since CP data serve as true reference for the optimization, fully corrected CP fluxes are crucial for the application of the correction (e.g., data processing or software). Different factors such as type of instruments, length of inlet tubing, tube diameter, and flow rate (see section 2.1) will systematically affect corrections of CP fluxes [*Aubinet et al*., 2016, 2012; *Burba and Anderson*, 2010a; *Metzger et al*., 2016]. For the CP system all applied corrections are seasonally independent, and thus, the CP system is used as a reference throughout the year. Furthermore, a correct application of the WPL density-flux correction [*Webb et al*., 1980] for the OP data is crucial, since otherwise a remaining bias would be projected on the self-heating correction. Here we applied all recommended correction and used standardized methods for the data processing [*Fratini and Mauder*, 2014] to ensure highest data quality.

### 2.4 Sonic Anemometer Heating and Icing Events

Using information from ancillary meteorological instrumentation, the sonic anemometer heating was controlled by the data logger and was activated (heater switched on) based on combined *rH* (>85%) and $T_a$ (<1°C) conditions. This heating scheme was designed to avoid icing and riming on the transducers. Documented icing events occurred during deactivated heating periods before, during, or after the icing events. Following an icing event, ice was either removed manually by the site technician after the detection or may have disappeared due to sublimation. This can alter the residence time and might cause differences in the icing event length between sonic anemometers, shorten icing events even if conditions would continue to promote icing, or lead to icing at individual sensors.

Since the same heating schemes were applied at both towers, and both towers experienced almost identical meteorological conditions, the sonic anemometer heating should be activated synchronously at both towers. Due to a reset of sonic anemometer setup parameters, the sonic anemometer heating was shut down and excluded from the heating activation protocol (hereafter referred to as nonheated) for two periods (tower 2: mid-October 2013 to April 2014; tower 1: mid-January to May 2015), while at the other tower the heating was controlled by the data logger and activated based on meteorological conditions (hereafter referred to as controlled-heating). Thus, during these phases conditions between nonheated sonic anemometer and the sonic anemometer with controlled heating can be compared for cases with activated heating (e.g., controlled-heating activated) and without heating at both sonic anemometers. For reasons of data quality assessment, the data analysis of the heating effect for the first period was restricted until the end of 2013 (Figure 1). Heated and unheated

conditions are compared during both winter seasons by combining data from both observation systems (e.g., heated conditions represent data from tower 1 during the first winter season and data from tower 2 during the second winter season). It is assumed that during the polar winter with a closed snow cover, variability in microsite conditions between the towers can be neglected. In total 26 weeks are available for an in-depth analysis of the sonic anemometer heating.

For the identification of potential icing events, error messages given by the sonic anemometer were analyzed. Error messages were recorded with a frequency of 20 Hz and stored additionally to the high-frequency EC data in an extra file and were counted per half-hour interval for the same temporal resolution as for EC data without distinguishing between individual error messages. These additional data logs indicate potential disturbance or blockings of the sonic anemometer signal. Icing events were identified as periods with the maximum number of error messages per half hour (36,000), indicating a "permanent" disturbance of measurements that is unlikely to be caused by short-term meteorological conditions. Since EC data during icing events are inaccurate ancillary measurements are used to characterize meteorological conditions.

# 3 Results

## 3.1 Self-Heating of Open-Path Sensor

### *3.1.1 Differences Between Non-Self-Heating Corrected Open-Path Gas Analyzer and Closed-Path Reference Data*

Wintertime $CO_2$ fluxes obtained from the OP and CP were correlated ($r = 0.97$, $N > 5700$) showing that both measurement systems generally capture the same signal. With an orthogonal regression analysis (CP = Intercept + Slope · OP) an intercept of −0.284 (−0.294 to −0.274 as 95% confidence interval) μmol $m^{-2}$ $s^{-1}$ and a slope of 1.142 (1.135–1.150 as 95% confidence interval) were obtained. A negative intercept indicates that the OP has the tendency toward more negative $CO_2$ fluxes, i.e., more uptake by the ecosystem. Even under cold ambient conditions with completely frozen soils and monthly mean $T_a$ below −30°C (December–February) where active assimilation of $CO_2$ by the ecosystem is virtually impossible, average $CO_2$ fluxes ranged around or below zero with the operation of an OP (−0.18 ± 0.71 μmol $m^{-2}$ $s^{-1}$), while the reference CP shows positive mean $CO_2$ fluxes (0.19 ± 0.4 μmol $m^{-2}$ $s^{-1}$; see Figure S1 in the supporting information).

These observations suggest a systematic bias in OP measurements that can only be clearly demonstrated during wintertime, since no other influence factors (e.g., uptake by meteorological or biological forcing) besides instrument self-heating can cause negative flux rates. However, carbon dioxide flux offsets between OP and CP systems show similar tendencies over the full annual cycle (Figure 2a), resulting in a cumulative offset of 96 gC $m^{-2}$ for the data year 2015. Discrepancies in net flux rates between the OP and the CP were found to have different gradients for different seasons:

1. Winter: Strong offsets between OP and CP fluxes were observed in the period December through February. These differences already amount to 17 gC $m^{-2}$ in the first months of the year (January–February, period 1 in Figure 2b). In December, the

CP shows higher positive fluxes adding another 12 gC $m^{-2}$ to the observed differences (period 5 in Figure 2b).

2. Transition seasons: During the last months of winter toward spring (March through May, period 2 in Figure 2b) and in fall (October, period 4 in Figure 2b) flux rates between OP and CP generally agree; thus, no systematic differences are observed. Accordingly, in this period the offset between the two GAs remains nearly constant.
3. Summer: Large differences arise again during the season from June to September (period 3 in Figure 2b) with the OP showing higher uptake rates. As a result, the gap in cumulative fluxes between OP and CP steadily increases, summing up to 57 gC $m^{-2}$ for this season.

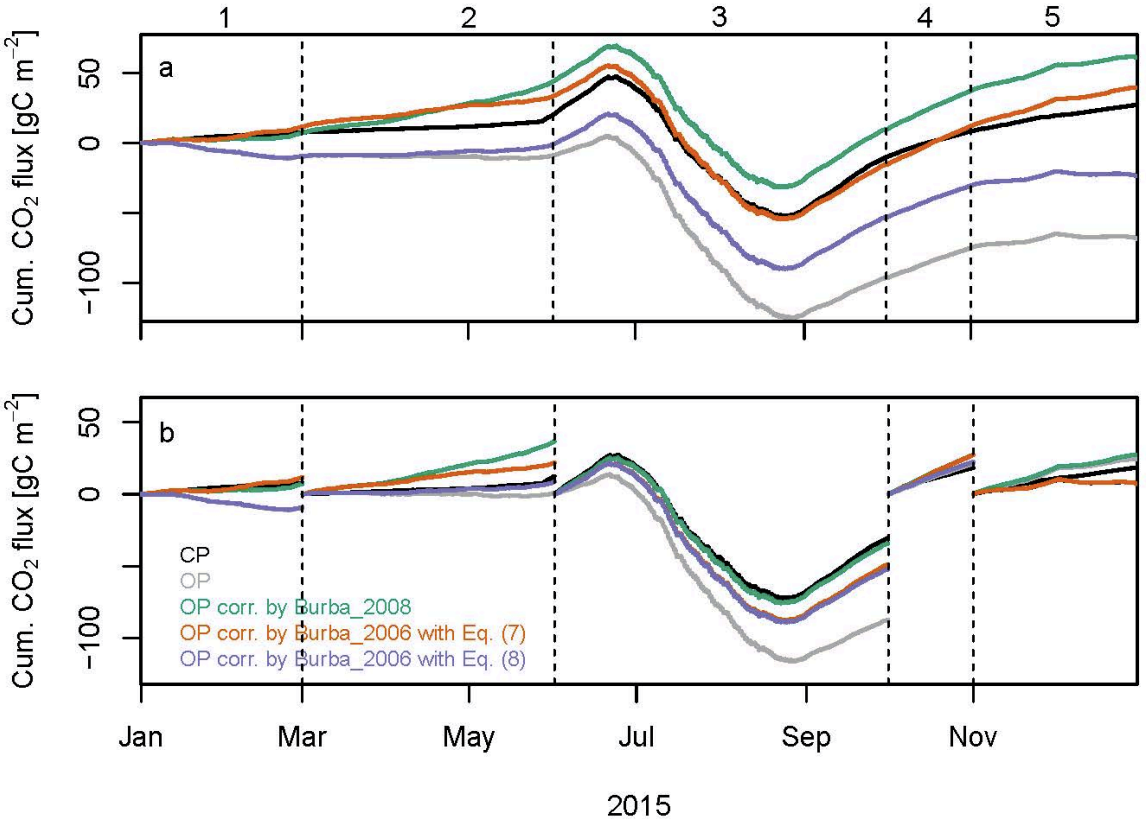


**Figure 2.** Comparison of cumulative CO2 fluxes for the CP (black) and OP (gray) systems and different approaches of the self-heating correction for the OP (colored lines) calculated for (a) a full year and (b) per season.

### *3.1.2 Application of the Self-Heating Correction Scheme*

The apparent enhancement in net uptake of $CO_2$ as measured by the OP is likely to be caused by the self-heating of the instrument linked to the additional heat flux within parts of the optical path disturbing the measurements [*Burba et al.*, 2006, 2008]. The aim of the self-heating correction is to eliminate the self-heating effect of the OP and thus reduce the differences between both GAs.

To analyze the performance of the correction, an orthogonal regression analysis is performed before and after the application of the correction with the intercept representing the offset (Table 3). Different linear relationships between $CO_2$ fluxes from OP and CP reference during

daytime and nighttime (Table 3) are observed. Therefore, $\xi$ fractions were fitted separately for daytime and nighttime conditions (Table 2). Fitted $\xi$ during day are by a factor of 3 to 7 larger than during the night. Fitted $\xi$ are tightly linked to the correction approach with $\xi$ varying between 0.1 (Burba_2006) and 0.8 (Burba_2008). This variation is attributed to systematic differences in the formulations, i.e., equations 3 and 6. Fitted $\xi$ <1 indicate that with an inclined OP analyzer the required correction is always less than what was suggested for vertically mounted instruments. Intercepts after the self-heating correction stay above zero for the Burba_2006 approach, indicating that there are remaining flux patterns that cannot be corrected for. For the Burba_2008 approach a negative intercept during daytime indicates a significant overcorrection.

**Table 3**. Overview of Results From Nonlinear Fit for the Fraction $\xi$ With *Burba et al*. [2008] as Equation 4 With Equation 3, *Burba et al*. [2006] as Equation 5 With Equation 7, and *Burba et al*. [2006] as Equation 5 With Equation 8 [a].

| Time of day | Self-heating correction approach | $\xi$ | Intercept [μmol $m^{-2}$ $s^{-1}$] | Slope | $r$ |
|---|---|---|---|---|---|
| Daytime | no correction | - | -0.427 (-0.459 – -0.396) | 1.111 (1.100 – 1.122) | 0.96 |
| | Burba_2008 | 0.806 ± 0.017 | 0.247 (0.201 – 0.294) | 1.084 (1.067 – 1.101) | 0.98 |
| | Burba_2006 with equation (7) | 0.130 ± 0.004 | -0.061 (-0.113 – -0.007) | 1.115 (1.095 – 1.135) | 0.97 |
| | Burba_2006 with equation (8) | 0.077 ± 0.002 | -0.066 (-0.118 – -0.013) | 1.121 (1.101 – 1.140) | 0.97 |
| Nighttime | no correction | - | -0.297 (-0.327 – -0.268) | 1.242 (1.210 – 1.278) | 0.81 |
| | Burba_2008 | 0.294 ± 0.026 | -0.150 (-0.215 – -0.100) | 1.214 (1.141 – 1.292) | 0.83 |
| | Burba_2006 with equation (7) | 0.042 ± 0.003 | -0.129 (-0.196 – -0.067) | 1.214 (1.139 – 1.295) | 0.82 |
| | Burba_2006 with equation (8) | 0.011 ± 0.006 | -0.264 (-0.328 – -0.204) | 1.179 (1.107 – 1.256) | 0.82 |

[a] Slope and intercepts are obtained from orthogonal regression analysis, CP = Intercept + Slope OP. Values in parentheses indicate the 95% confidence interval of the parameter estimates obtained for slope and intercept. Pearson's correlation coefficients ($r$) are given in the last column. Data cover two full annual cycles from April 2014 to 2016.

To evaluate the performance of the self-heating correction approaches, corrected cumulative $CO_2$ budgets were compared to the CP reference (Figure 2). Residual differences remain after the self-heating correction, with gradients of cumulative deviations to the reference varying by season:

1. Winter: For both periods 1 and 5 in Figure 2b, the self-heating correction approach by Burba_2006 with equation 8 has nearly no impact on the fluxes and patterns remain close to the input signal. Under nighttime conditions, temperature differences between ambient air temperature and estimated $T_s$ are small with equation 8, resulting in a

negligible $\xi$ (Table 3) and therefore no substantial self-heating correction. The correction approach with Burba_2008 and Burba_2006 with equation 7 yielded good agreement with the CP reference.

2. Transition seasons: During spring (period 2 in Figure 2b) the self-heating correction approach by Burba_2008 is strongly overcorrecting the $CO_2$ fluxes leading to a cumulative difference of 24 gC $m^{-2}$ in comparison to the CP reference. A slight overcorrection is also found with the Burba_2006 with equation 7 approach, while corrected $CO_2$ fluxes with Burba_2006 and equation 8 agree with the CP reference. In contrast during fall (period 5 in Figure 2b) all correcting approaches show comparable results and seem to slightly overcorrect $CO_2$ fluxes.
3. Summer: In period 3 (Figure 2b), with largest differences between OP and CP (see section 3.1.1), the Burba_2006 approach, independent of the $T_s$ parameterization, is undercorrecting the $CO_2$ flux with differences of maximal 22 gC $m^{-2}$. The correction approach with Burba_2008 yielded good agreement with the CP reference.

Overall, in 2015, cumulative annual difference to the CP reference are −34, −12, and 51 gC $m^{-2}$ for the self-heating correcting approaches Burba_2008, Burba_2006 with equation 7, and Burba_2006 with equation 8, respectively. This indicates that independent of the correction approach, the self-heating correction cannot fully remove the offset or is overcorrecting the OP signal. The self-heating correction is only accounting for an overall intercept, capable of removing a net bias while being unable to change the shorter-term flux patterns. Still, even for those cases, small seasonal fluctuations remain that lead to nonzero offsets, which may be linked to large seasonal differences between CP and the OP signal, differences between daytime and nighttime conditions, and also the method itself might be subject to methodological uncertainties (details in Appendix A).

### *3.1.3 Implications of the Self-Heating Correction on $CO_2$ Budgets*

The approaches that yielded best results on an annual scale (Figure 2 and section 3.1.2), e.g., Burba_2008 and Burba_2006 with equation 7, are used to apply the self-heating correction and offset the self-heating effect of the OP analyzer. With this self-heating correction for the OP, $CO_2$ fluxes are shifted toward less negative and more positive fluxes. Formerly negative or close to zero wintertime $CO_2$ fluxes now show a distinct positive mean value (Figures 3a and 3b). In summer, the $CO_2$ loss is increased, and therefore, the net uptake is reduced. Results corrected for the self-heating are much closer to the reference CP fluxes (Figures 3a and 3b) than results without the application of this additional correction.

Still, systematic discrepancies remain within individual seasons; e.g., in winter some of the weekly mean flux rates remain close to zero or in the negative range, even though absolute values are small. Overall, both approaches of the self-heating correction overcorrect OP fluxes during winter, and undercorrect them in summer (see intercepts in Table 2 and cumulative $CO_2$ budgets in Figures 3c and 3d). The residuals between corrected OP and CP reference during summer and winter partly balance each other for both self-heating correction approaches. With the Burba_2008 approach differences to the CP reference during summer and winter are marginal, but annual differences account to 34 gC $m^{-2}$, induced by the transition period in spring (Section 2 in Figure 2). In comparison the Burba_2006 approach with equation 7 shows higher summer and winter residual but a closer agreement on annual scale (12 gC $m^{-2}$).

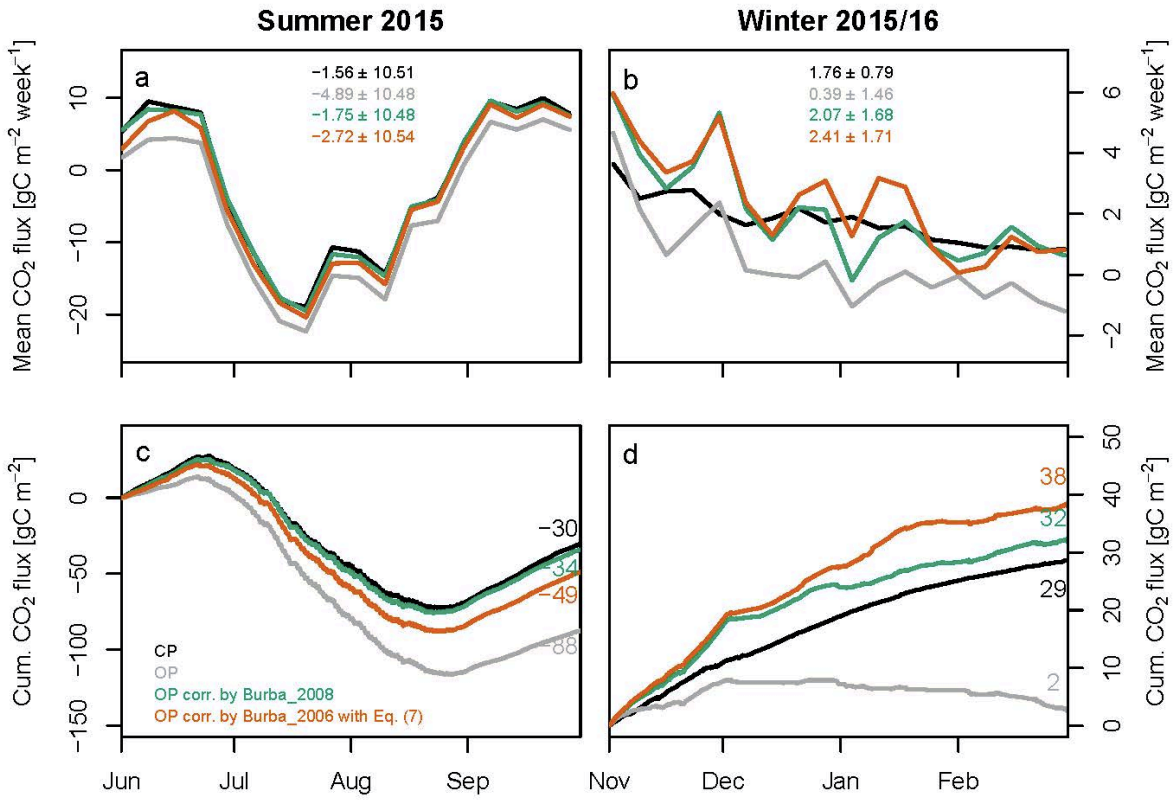


**Figure 3.** (a and b) Weekly averaged fluxes with mean flux rates (top center as mean ± standard deviation (µmol $m^{-2}$ $week^{-1}$)) and (c and d) cumulative budgets with seasonal budgets ((gC $m^{-2}$), with number representing seasonal budgets with corresponding color coding). Figures 3a and 3c give results for the summer season 2015 (June–October) and Figures 3b and 3d for the following winter 2015/2016 (November–March). Note that axes for summer and winter are different due to systematically different flux rates for each season.

### *3.1.4 Components of the Self-Heating Correction Approaches*

For the application of the self-heating correction a combination of input parameters is required with different magnitudes and seasonal courses. In the discussion to follow, we compared the approaches Burba_2008 and Burba_2006 with equation 7 to analyze the relative influence of individual components of the self-heating correction. The self-heating correction in total has a pronounced seasonality (Figures 4a and 4b). By separating into individual terms (Figures 4c and 4d), it can be demonstrated that single terms can have diverse dynamics over the course of a year.

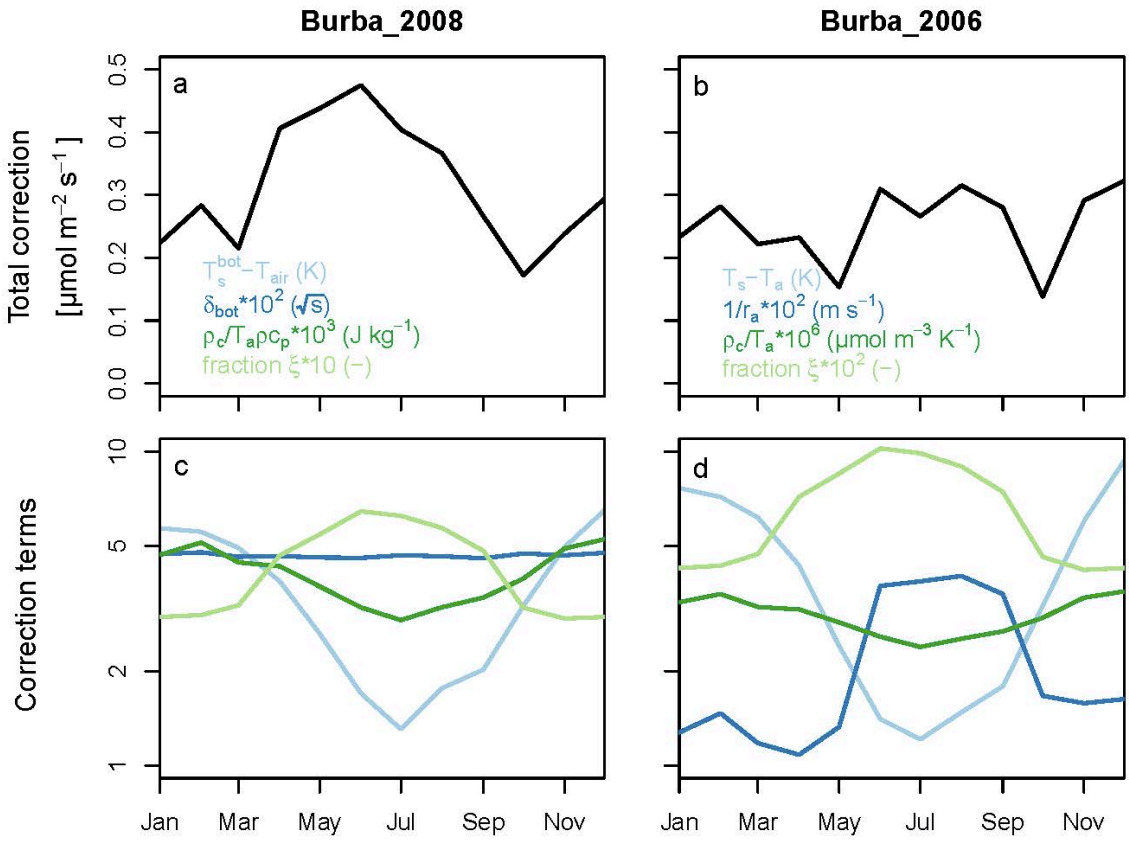


**Figure 4.** Monthly means for self-heating correction approaches (a and c) Burba_2008 and (b and d) Burba_2006 (right) in total (Figures 4a and 4b) and for individual terms with a logarithmic scaling (Figures 4c and 4d). The legend in Figures 4a and 4b described the color coding in the corresponding bottom panel. The seasonal variability of the fraction $\xi$ is caused by the varying proportions of daytime and nighttime over the course of the year, since the values optimized for daytime conditions are significantly higher than those for nighttime. For the Burba_2008 approach only the parameterization from the bottom part of the sensor is used, because the top and spars section only have a marginal influence on the overall correction.

In both correction approaches the temperature gradient between the ambient air and the surface of the sensor (light blue lines in Figures 4c and 4d) is a crucial part. While it is directly implemented in the Burba_2006 approach, it is used to estimate the sensible heat flux in the Burba_2008 approach. The seasonality of the temperature gradient is comparable in both approaches, but absolute values differ because of different offsets in the parameterizations. A second important element of the self-heating correction is focusing on the turbulent conditions. The Burba_2008 approach is using a geometric estimation with the average thickness of the boundary layer ($\delta$; dark blue line in Figure 4c) that stays relatively stable over the course of the year. For the Burba_2006 approach it is represented as the reciprocal of aerodynamic resistance (dark blue line in Figure 4d) with a strong increase in May and decrease in September with quasi-flat stages in-between, strongly influenced by the friction velocity. The third term of the self-heating correction composed of the densities (dark green line in Figures 4c and 4d) is slightly different for both approaches, but since there is no notable dynamic in the seasonal course, there is no systematic effect on the overall correction. A seasonality of $\xi$ (light green lines in Figures 4c and 4d) is caused by the separation into daytime and nighttime conditions representing summer and winter, respectively. While higher

absolute values are found in the Burba_2008 approach the relative changes over the year are similar for both correction approaches (Table 3).

In total, the seasonal dynamic of the Burba_2008 approach results from the temperature gradient and the $\xi$ fraction (Figure 4a). For the Burba_2006 approach the total correction is dominated in winter by the temperature gradient and the summer maximum is caused by the second term (Figure 4b). Differences between approaches emerge around March/April, with stable to slightly decreasing tendencies for the total correction with the Burba_2006 approach due to decreasing aerodynamic resistance while the total correction with the Burba_2008 approach is already strongly increasing, causing an strong overcorrecting (see period 2 in Figure 4).

### 3.2 Heating of Sonic Anemometer

The scheme based on meteorological conditions ($rH$ and $T_a$) to control the activation of the sonic anemometer heating worked as planned for the sonic anemometer with controlled-heating and was always switched on when corresponding meteorological threshold conditions were reached. In total 1365 and 849 half-hour intervals with active heating for winter 2013/2014 and winter 2015 as well as 6387 and 4449 half-hour intervals without heating for winter 2013/14 and winter 2015, respectively, are observed (Figures 5a and 5b). Air temperature during both winter periods is almost always below 1°C; therefore, $rH$ is the driving parameter for controlling the sensor heating. Monthly means for $rH$, averaged over both winter seasons, are highest during October, November, and December (82%). Accordingly, periods with active heating occur more often during winter 2013/2014 covering October, November, and December with most humid conditions and active heating for 26–33% of the time. An exception is April 2015 with large fluctuations in $rH$, resulting in an overall low mean but activated heating around nearly one quarter of the time.

During the first winter period (2013/2014), continuous error messages were observed for both sonic anemometers more or less simultaneously in January 2014 (Figure 5a). During this time, air temperatures dropped mostly below −40°C, i.e., outside of the measuring range of the sonic anemometer; thus, it cannot be determined if low temperatures or icing of the sensor was triggering these error messages. Therefore, the period of January 2014 was excluded and the focus was set to December 2013.

In mid-December 2013 (Figure 5c), sustained high frequency (around 36,000 error messages per half hour) of error messages were observed at the nonheated sonic anemometer, indicating icing of the sensor over duration of several hours. For the same period, at the sonic anemometer with controlled-heating and activated heater error messages are scattered and small (<550 error messages per half hour). This demonstrates that icing has been prevented by the sonic anemometer heating while without this heating ice could build up and disturb instrument performance. We assume that the icing at the nonheated sonic anemometer was eventually removed manually by the site technician, since it appeared only for a very short time period, while meteorological conditions did not change substantially during this event.

In the second winter period (2015) both sonic anemometers showed high error message counts independently from each other. The icing in both cases lasted for a more extensive period (2–3 days) for both the nonheated sonic anemometer and the sonic anemometer with controlled-heating, respectively (Figure 5d). We hypothesize that the ice buildup event which occurred during activated heating in late January 2015 might have been caused by icing fog

introducing riming. The second ice buildup during the second winter period (mid-February 2015) only occurred at the nonheated sonic anemometer. The previous discontinuous heating at the sonic anemometer with controlled-heating switched off 3 h before the ice buildup started at the nonheated sonic anemometer. We assume that the heating prevented the initial stages of ice buildup at the heated tower, so even though the heating was not running at the time the ice finally closed around the nonheated sensor, it can be assumed that the active heating made the difference in this case.

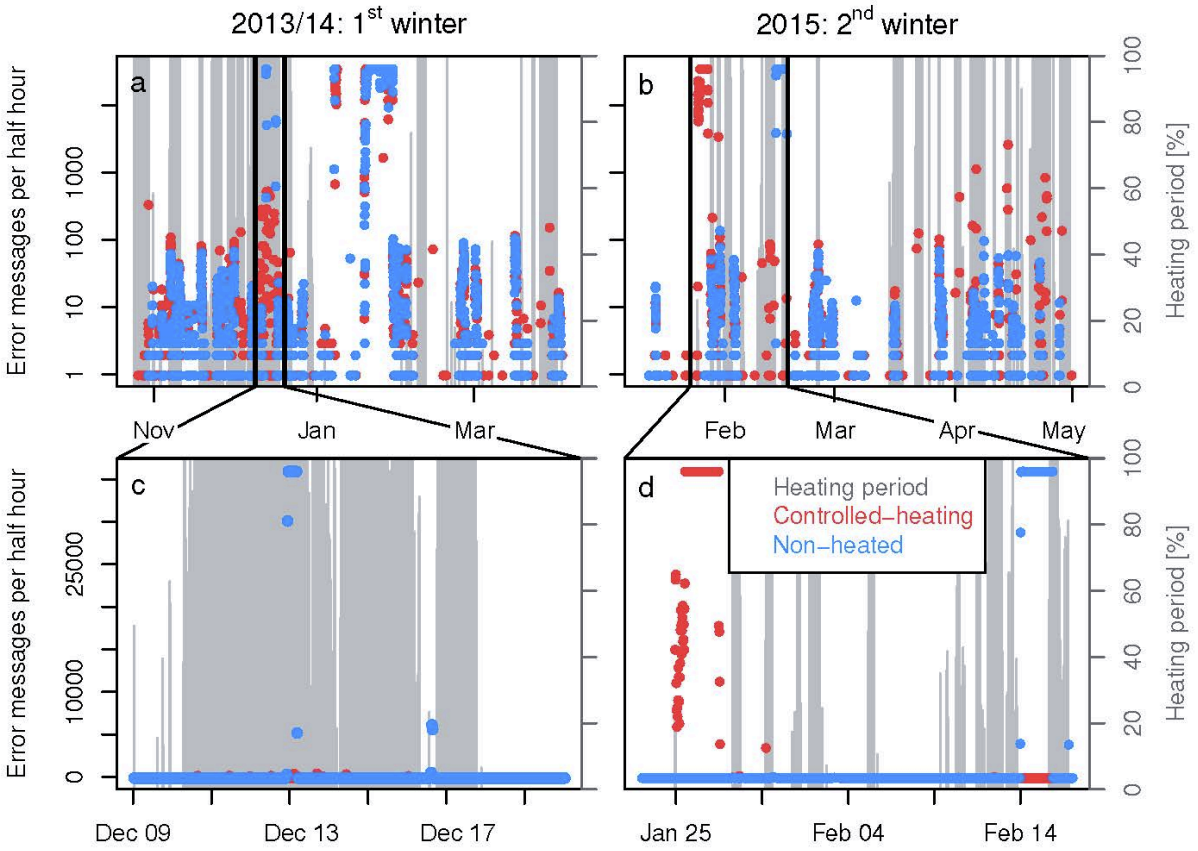


**Figure 5.** (a–d) Heating periods (gray bars) and recorded error messages from the sonic anemometers (red and blue symbols) during both winter seasons. The vertical size of the gray bars depicts the fraction of each half-hour interval with activated heating (right axis), and the symbols show the number of error messages (left axis) at the sonic anemometer with controlled-heating (red symbols) and at the nonheated sonic anemometer (blue symbols). Figures 5c and 5d focus on a more detailed period that is marked with black bars in Figures 5a and 5b (note the changes of the *y* axis from logarithmic to linear scale from the top to the lower panel).

### *3.2.1 Heating Effect on Sensible Heat and Momentum Fluxes*

Without heating, differences in mean $T_a$ averaged for both sonic anemometers are close to zero with 0.2°C and −0.3°C for the first and second winter periods, respectively (Figures 6c and 6d and see Figures S2c and S2d). With activated heating, there is a systematic shift in $T_a$ measured by the sonic anemometer with controlled-heating in comparison to the nonheated sonic anemometer (Figures 6a and 6b) as well as to the ancillary sensor (see Figures S2a and S2b). The $T_a$ difference between both sonic anemometers increased slightly over time (first winter: −1.5 K; second winter: −1.9 K), resulting in a mean $T_a$ reduction of approximately −1.8 K as a consequence of sensor heating.

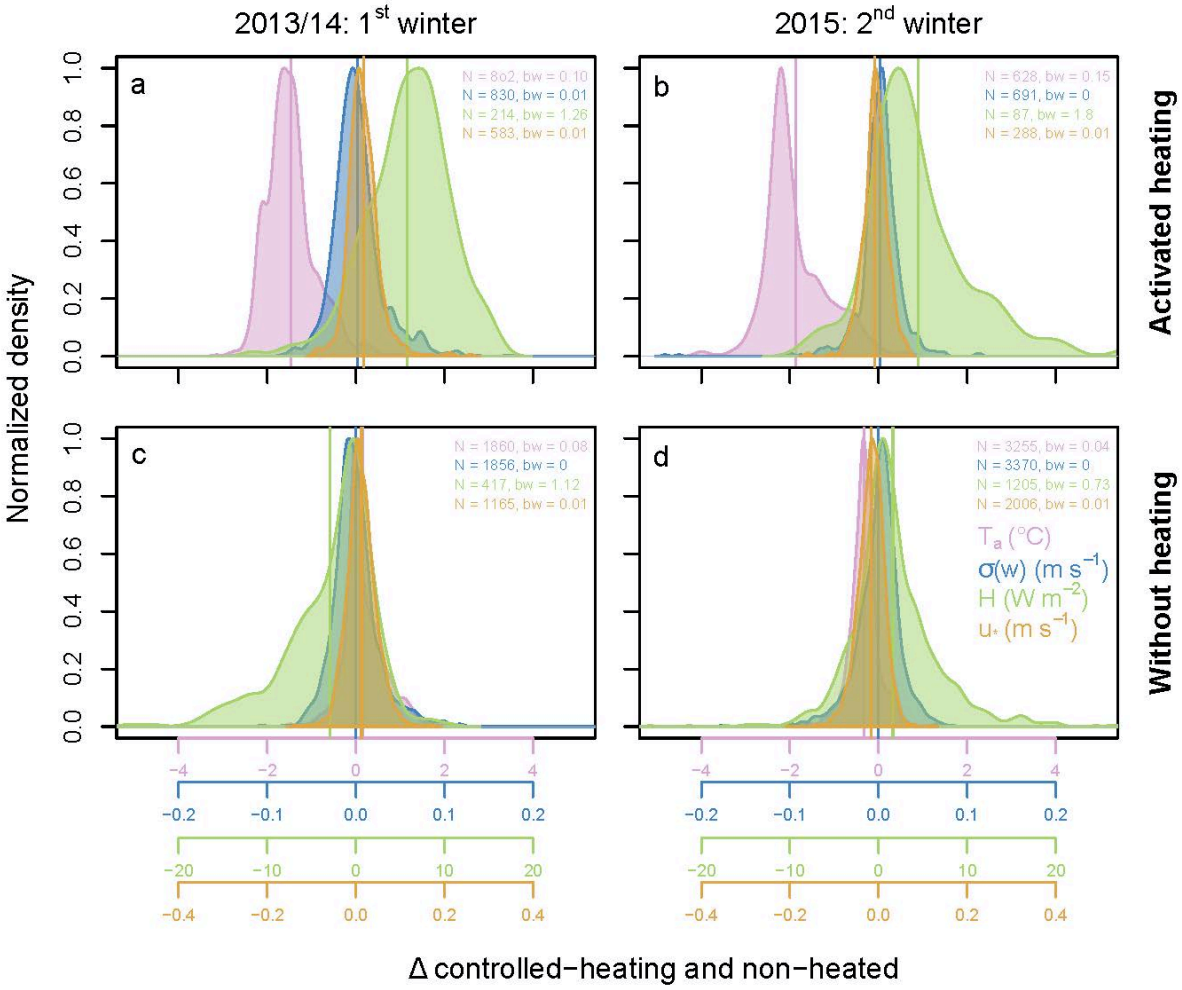


**Figure 6.** Comparison of differences of air temperature ($T_a$, purple), variance of the vertical wind speed ($\sigma^2(w)$, blue), sensible heat flux ($H$, green), and friction velocity ($u_*$, orange) retrieved from the sonic anemometer for both winter periods: (a and c) the first winter season and (b and d) the second winter season, with activated (Figures 6a and 6b) and without (Figures 6c and 6d) heating. Total number of data ($N$) and bandwidth (bw) of the kernel density estimation for each variable and heating-case are given in corresponding colors in each subplot. Note that each variable has its own color-corresponding $x$ axis and that ranges between $x$ axes differ. Densities were normalized by their range. The vertical lines indicate means.

Differences in the sensible heat flux between both sonic anemometers during periods without heating are close to zero, with median values of $-2.9$ W m$^{-2}$ and 1.6 W m$^{-2}$ (Figures 6c and 6d), for the first and second winter periods, respectively. With activated heating, sensible heat fluxes tend to increase, with mean offsets of 5.8 W m$^{-2}$ and 4.5 W m$^{-2}$, for the first and second winter periods, respectively. Overall, we found an increase in sensible heat fluxes of 5.2 W m$^{-2}$ with activated heating.

Since double axis rotation is applied within the flux-processing software, implications of the sonic anemometer heating on the fluctuations of the vertical wind component can only be investigated by analyzing $\sigma(w)$. Negligible differences between both sonic anemometers are observed with activated ($0.002 \pm 0.030$ m s$^{-1}$ and $0.000 \pm 0.030$ m s$^{-1}$, as mean ± standard deviation) and without ($0.002 \pm 0.030$ m s$^{-1}$ and $-0.002 \pm 0.030$ m s$^{-1}$, mean ± standard deviation) heating (Figure 6), for the first and second winter periods, respectively. Consequently, only minor differences of sonic anemometer heating can be found also for the

friction velocity with activated (0.02 m $s^{-1}$ and −0.01 m $s^{-1}$) in comparison to conditions without (0.01 m $s^{-1}$ and −0.02 m $s^{-1}$) heating, for the first and second winter periods, respectively.

### *3.2.2 Heating Effect on the $CO_2$ Fluxes*

Carbon dioxide flux measurements based on the CP gas analyzing system are not affected by the sonic anemometer heating; i.e., mean $CO_2$ flux offsets between both EC systems with activated ($-1.6 \times 10^{-2}$ µmol $m^{-2}$ $s^{-1}$) and without ($-4.1 \times 10^{-3}$ µmol $m^{-2}$ $s^{-1}$) heating do not differ significantly ($p = 0.9704$, Mann-Whitney test; Figure 7). On the other hand, computing fluxes based on the OP gas analyzing system (corrected for the self-heating of the open-path analyzer by the Burba_2006 approach with equation 7), we observe a more pronounced sonic anemometer heating effect. The mean $CO_2$ flux is significantly ($p < 0.05$, Mann-Whitney test) shifted from 0.02 µmol $m^{-2}$ $s^{-1}$ without heating toward 0.21 µmol $m^{-2}$ $s^{-1}$ with activated heating (Figure 7), resulting in a mean increase in $CO_2$ fluxes of 0.19 µmol $m^{-2}$ $s^{-1}$. There is, however, no significant difference between $CO_2$ fluxes measured by both CP systems, and thus, site differences can be ruled out as a possible explanation. Assuming continuous operation of the sonic anemometer heating, this mean increase in $CO_2$ fluxes would sum up to an additional 30 gC $m^{-2}$ in wintertime efflux over the entire winter season (November – March).

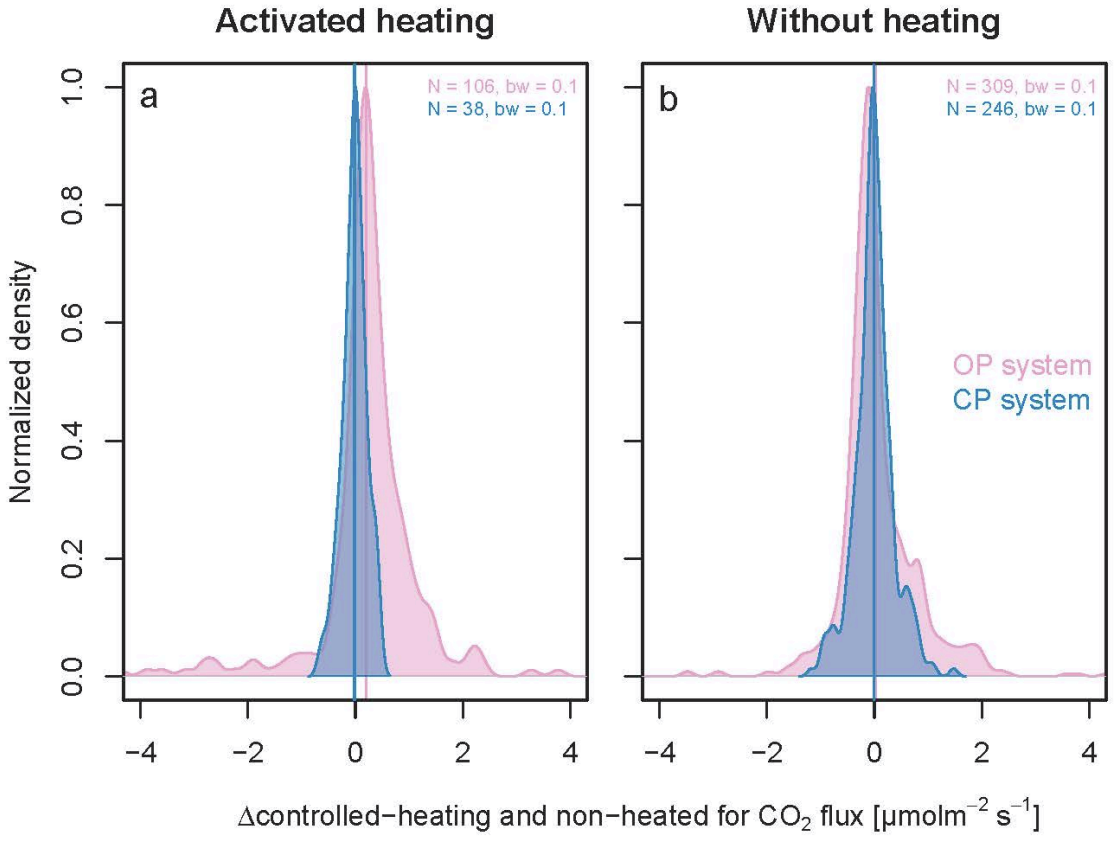


**Figure 7.** Comparison of NEE differences from the OP (purple, representing the first winter season 2013/2014) and CP (blue, representing the second winter season 2015) between (a) heated and (b) unheated conditions. Total number of data (*N*) and bandwidth (bw) of the kernel density estimation for each variable are given in corresponding colors in each subplot.

The fact that systematic shifts in fluxes were only observed when calculating fluxes based on OP data suggests an indirect heating effect that can be attributed to the WPL density-flux correction [*Webb et al*., 1980]. This correction, applied to OP gas analyzers, includes air temperature and sensible heat flux as input data. Accordingly, biases in those will indirectly influence density-corrected OP $CO_2$ fluxes via this correction. In a sensitivity study, we found that the net bias was almost exclusively caused by offsets in sensible heat fluxes, while systematic shifts in the air temperature caused negligible net effects in the $CO_2$ fluxes.

# 4 Discussion

## 4.1 Self-Heating of the Open-Path LI7500 Sensor

The apparent enhancement in net uptake of $CO_2$ with 96 gC $m^{-2}$ as measured by the OP is likely to be caused by the self-heating of the instrument linked to the additional heat flux within parts of the optical path disturbing the measurements [*Burba et al*., 2006, 2008]. *Järvi et al*. [2009] determined a 140 gC $m^{-2}$ difference between an OP and CP during roughly 2 months (October–December) for a beech forest site in Finland. However, their data were not gap filled, and the study time frame is very short in comparison to the data presented here. If no reference measurements are present, the potential uptake that may be caused by self-heating of the sensor can be estimated by comparing flux differences between the OP sensor with and without the self-heating correction. Based on this concept, existing studies found differences of 20 gC $m^{-2}$ [Barrow, *Ueyama et al*., 2012] and 87 gC $m^{-2}$ (Atqasuk [*Oechel et al*., 2014]) per year at two Alaskan sites representing similar environmental conditions as our sites near Chersky. *Reverter et al*. [2011] identified a linear fit between mean annual temperatures and the net effect of the self-heating correction, where the correction effect was clearly elevated at sites situated in cold regions. Applying their suggested approach with a mean temperature of −11°C found in Chersky [*Kittler et al*., 2016] suggests a reduction of the $CO_2$ uptake of 240 gC $m^{-2}$ through application of the self-heating correction. This apparent overcorrection can be explained by the fact that environmental conditions in Chersky (e.g., annual mean temperature and ecosystem type) are far outside the range analyzed by *Reverter et al*. [2011]. Accordingly, our findings indicate that the linear fit between magnitude of the self-heating correction and prevalent temperature cannot be applied across a broad temperature range and that instead nonlinear elements (e.g., wind speed, wind direction, and mounting of the analyzer) need to be included when extending the approach by *Reverter et al*. [2011] to the Arctic domain.

The greatest impact of the self-heating is expected during winter with lowest air temperatures and hence relative highest contribution of the heating effect to the total sensible heat fluxes [*Burba et al*., 2008; *Grelle and Burba*, 2007]. This theory is supported by some existing studies that achieved a good agreement between OP and reference measurements during the growing season [*Goodrich et al*., 2016]. However, other references demonstrate that the self-heating effect is not only affecting fluxes during the cold season, but corrections for sensor self-heating have to be applied to warm season measurements as well [*Järvi et al*., 2009; *Ueyama et al*., 2012], with different magnitudes in the heating effect [*Reverter et al*., 2011]. *Oechel et al*. [2014] found similar seasonal patterns as observed in the presented study, i.e., with high impact of self-heating during both summer and winter seasons, while spring and fall provide just minor contributions to offsets in cumulative flux budgets.

Since different linear relationships between $CO_2$ fluxes from the OP and the CP can be observed during daytime and nighttime conditions, the $\xi$ fractions were fitted separately. The closer agreement during nighttime is also reflected by some instrument surface temperature estimations with systematically lower offsets during nighttime. Radiative heating over the day and radiative cooling during the night can affect measurements, and this effect might be increased under nonvertical OP sensor configurations [*Burba et al*., 2008] as it is used in this study. This has implication on the fitted $\xi$ that are an order of magnitude smaller under nighttime conditions, compared to the daytime fits. Since our study site is situated in the Arctic, this difference leads to a $\xi$ fraction seasonality in the overall self-heating correction, because the fractions of daytime and nighttime vary strongly between summer and winter seasons, respectively.

For all self-heating correction a strong dependency of $\xi$ on the approach and the parameterization of the instrument surface temperature was demonstrated.

1. In case of the Burba_2008 approach with equations 4 and 3, negligible differences in cumulative $CO_2$ fluxes in comparison to the CP are observed during summer and winter. Annual differences to the CP system are 34 gC $m^{-2}$, due to an overcorrection during the spring. In general, the Burba_2008 approach represents the most complex structure, dividing the sensor into different sensor elements. The approach was derived for a fully vertical sensor position [*Burba et al*., 2008], and an adjustment for inclined sensor mounting is described in *Oechel et al*. [2014] by tuning the temperature parameterization of the bottom part of the sensor. Here we used a different adjustment by introducing the $\xi$ fraction. Relatively high $\xi$ factions, for both daytime and nighttime conditions with equation 4, in comparison to equation 5 implying that the correction approach itself can already correct for a large fraction of the sensors self-heating without major tuning, especially under daytime conditions.
2. The Burba_2006 approach with a combination of equations 5 and 7 results in negligible differences in comparison to the CP in the annual cumulative $CO_2$ fluxes caused by counteracting tendencies with an overcorrection during winter and an undercorrection during summer. For another study this method with an empirically determined $\xi$ of 0.05 yielded reasonable results [*Rogiers et al*., 2008]. During nighttime, absolute values of $\xi$ fits from the presented study agree with this finding, but under daytime conditions the value is 3 times higher. This difference may be explained by the overall colder temperatures in Chersky, which imply a higher contribution of the self-heating.
3. While the apparent uptake during the Arctic winter is not corrected properly by using the Burba_2006 approach with equations 5 and 8, the fitted $\xi$ for daytime is comparable to the one for the Finnish beech forest [*Järvi et al*., 2009], achieving a good agreement with the reference measurements during the nonwinter season. Still, the overall fit of the annual correction is poor within the context of our study.

In general, both correction approaches equation 4 with equation 3 and equation 5 with 7 demonstrated a good performance, depending on the target aim. Annual $CO_2$ budgets yielded best results by applying equations 5 with 7 are performing best. If the focus is on correcting $CO_2$ fluxes during the main season e.g., summer and winter, best results were achieved with equation 4 with equation 3. Thus, further experiments with direct measurements of instrument surface temperature under natural conditions with different instrument configurations are necessary to improve the performance of estimates and reduce uncertainties. Furthermore, we found evidence that self-heating correction, in general, is influenced by flow patterns

indicating that the method is subject to methodological uncertainties that need further investigations.

### 4.2 Heating of Sonic Anemometer

Our results demonstrate that the chosen heating scheme can prevent ordinary ice buildup under expected meteorological conditions and in this way can reduce the power consumptions considerable below that of a continuous or intermittent heating strategy [*Goodrich et al*., 2016]. Still, there are special meteorological conditions, not being captured with this regular heating scheme, that can cause ice buildup and disturb measurements, like ice fog introducing riming as observed in late January during activated heating. Consequently, the riming should also appear at the unheated tower because of very similar meteorological conditions between sonic anemometers but might have been removed manually before major buildup started. Under this special meteorological situation, ice buildup cannot be anticipated by an activation scheme based on ancillary meteorological conditions. Accordingly, any such scheme to prevent sensor icing must fail.

In both existing studies focusing on the effect of sonic anemometer heating, continuous heating was found to increase the apparent sensible heat flux [*Goodrich et al*., 2016; *Skelly et al*., 2002], but a uniform explanation for this effect was not provided. Findings from this study suggest that temperature measurements from the heated sonic anemometer are the driving element for the observed differences in sensible heat fluxes, while the wind components only show a minor influence. The most likely explanation of the observed differences in $T_a$ with activated heating is an instrumental issue related to biases in sonic anemometer path lengths; i.e., heating of arms and transducers influences signal runtimes between the transducers. With an observed reduction in $T_a$ the path length is increased and that effect might be amplified under very cold environmental conditions.

Since no direct heating effect on the variability of the vertical wind speed and the resulting friction velocity was observed, it is also not expected to find a direct heating effect on the determined $CO_2$ mixing ratios and fluctuations. This assumption is confirmed by the finding that the activated heating does not lead to a shift in $CO_2$ fluxes based on the CP gas analyzing system. However, systematic indirect effects can occur when observations during activated heating (sonic temperature and sensible heat flux) are used as input for the WPL density-flux correction of OP flux measurements. In this context, shifts in sensible heat fluxes were found to be the major driver for a biased WPL correction when sonic anemometer heating is activated. The sonic anemometer heating holds the potential to significantly alter the seasonal $CO_2$ budget indirectly through biasing the WPL density-flux correction. The observed mean bias in $CO_2$ fluxes with active heating of this study is a magnitude larger than the overestimation reported by *Goodrich et al*. [2016] with $-0.03$ μmol $m^{-2}$ $s^{-1}$. The mean bias was found to be caused by a higher variance in the vertical wind component having a direct effect on the determined fluxes of $CO_2$ with a CP and the same type of sonic anemometer as used in this study [*Goodrich et al*., 2016].

### 4.3 Relevance of Wintertime $CO_2$ Budgets

At the site close to the city of Chersky that has been investigated in the context of this study, appropriately corrected wintertime emissions amount to about 30 gC $m^{-2}$. These net emissions are relatively low compared to the substantial net releases of $CO_2$ during wintertime which have been reported across different Arctic permafrost ecosystems like wet sedge

(115 gC $m^{-2}$), heath (99 gC $m^{-2}$ [both *Euskirchen et al*., 2012]), or forest tundra (89 gC $m^{-2}$ [*Zimov et al*., 1996]), all representing 3 years of measurements covering a period from September–April/May. Assuming a temperature dependence of winter $CO_2$ flux as suggested by, e.g., *Zimov et al*. [1996], shorter study time frames focusing on, e.g., just the core winter period might lead to smaller winter effluxes. Such results were presented, e.g., by *Oechel et al*. [2014] with 12 gC $m^{-2}$ covering a period from October to April for a moist acidic tundra or *Lüers et al*. [2014] with 6 gC $m^{-2}$ during November to April for a semidesert ecosystem. Given that the largest portion of wintertime $CO_2$ emissions observed at our site near Chersky can be attributed to the fall shoulder season and the transition into early winter, our observations generally agree with these findings but also indicate slightly higher efflux at the peak of polar winter than found at both of the other sites with continuous permafrost [*Lüers et al*., 2014; *Oechel et al*., 1997].

Since net $CO_2$ emissions during Arctic winter can sum up to a substantial portion of the growing season budget, correcting the self-heating of the open-path LI7500 gas analyzer and accounting for potential biases linked to the active heating of the sonic anemometer both are essential elements in the EC flux processing protocol to obtain high-quality annual budgets of $CO_2$ fluxes. In particular, neglecting the self-heating correction of the open-path gas analyzer would lead to a systematic low bias in wintertime emission estimates and accordingly would yield annual flux budgets with exaggerated net $CO_2$ uptake by the ecosystem [*Oechel et al*., 2014]. With future increases in Arctic temperatures expected particularly outside the growing seasons, it can be speculated that unfrozen soils will provide suitable conditions for decomposition of organic material for extended periods under future climate change, therefore further elevating the role of wintertime fluxes for annual $CO_2$ budgets. High-quality flux observations under the extreme conditions of polar winter are therefore essential for both assessing the role of Arctic ecosystems as net sources or sinks for greenhouse gases as well as for allowing a reliable quantification of changes in greenhouse gas fluxes as a consequence of climate change.

# 5 Conclusions

In this study, we quantified the effect of different heating systems to achieve high-quality year-round EC $CO_2$ fluxes in cold environments. The first part focused on the correction of the self-heating effect of the open-path gas analyzer, while the second part deals with the effect of the sonic anemometer heating on the determined scalars and fluxes. Based on our analyses of 3 years of continuous EC measurements from a site close to the city of Chersky, measures to avoid heating biases were developed, resulting in appropriately corrected wintertime emissions of about 30 gC $m^{-2}$. The methods we developed to avoid biases of instrument LI-7500 self-heating and controlled sonic anemometer heating on flux data quality were the following:

1. A self-heating correction for $CO_2$ fluxes based on the LI-7500 gas analyzer is essential to avoid systematic biases in long-term budgets. For an inclined sensor setup, not the full self-heating correction as proposed by *Burba et al*. [2008] needs to be applied.
2. Strongest self-heating biases in LI-7500 flux data were found not only in winter but also during the summer, while shoulder seasons were largely unaffected. Accordingly, self-heating correction not only needs to be applied for cold-season observations but is also essential for summertime $CO_2$ fluxes. Therefore, a year-round application of self-heating correction is necessary to avoid systematic bias on annual flux budgets.

3. Sonic anemometer heating affects measurements of sonic temperature and sensible heat fluxes, but no direct effect on the variability of the vertical wind speed and the resulting friction velocity was observed.
4. $CO_2$ fluxes based on a CP gas analyzer are unaffected by sonic anemometer heating, and longer heating periods are likely to have a positive effect on the data quality of these fluxes. A small but systematic indirect bias of sonic anemometer heating on $CO_2$ flux data occurs through the application of the WPL density-flux correction for open-path analyzers, since this correction scales with the sensible heat flux, which is biased when the heating is activated. For the OP fluxes a shorter but recurring application of heat pulses to avoid icing of the sensor may prove beneficial for eddy-covariance flux data quality in cold climates, particularly if icing fog events can occur

We recommend a sonic anemometer heating scheme for Arctic conditions that is not controlled by meteorological conditions, but instead either is activated at regular intervals independent of prevailing weather conditions or use extended heating periods up to permanent heating. For the first option possible solutions might be to activate the sonic anemometer heating for an hour per day in staggered cycles to avoid preferentially exclusion of a specific period while removing potential icing to guarantee high-quality measurements. However, a strong disturbance of the observed turbulent fluxes takes place during activation/deactivation periods of the sonic anemometer heating, so these transition periods need to be flagged as lowest data quality and discarded from further flux data analysis. If an OP system is used, $CO_2$ fluxes should be treated with caution due to the indirect heating effect of the sonic anemometer. Accordingly, to avoid systematic biases in the OP $CO_2$ budget, either an alternative data source for the sensible heat flux (e.g., ancillary instrumentation or gap-filling) needs to be used as input for the WPL density-flux correction or a suitable correction procedure to minimize the systematic offsets in sensible heat fluxes during sonic anemometer heating periods should be applied.

# Appendix

Sensor geometry might be a crucial component if the OP sensor is mounted in an inclined position (Figure A1a), while it should be independent for vertically oriented instruments [*Burba et al*., 2008]. For different directions of the horizontal wind, heated air might be blown further into (Figure A1b) or out of (Figure A1c) the optical path, with potential consequences for the impact of the self-heating effect and therefore also on the necessary correction. To investigate the dependence of $\xi$ on the wind field properties, equation 5 with equation 7 was reorganized to determine $\xi$ directly for each half-hour interval and subsequently deriving statistics on the dependence of the $\xi$ fraction for certain wind direction and wind speed classes. Since this approach does not account for nonlinear dependencies by minimizing the sum of squared residuals, values can vary systematically in comparison to the optimization approach. Accordingly, this analysis will only be used to identify how the sensor geometry and the angle of attack can influence the self-heating correction.

To investigate the dependence of the sensor geometry and wind fields on the self-heating correction, $\xi$ was computed individually for each 30 min interval ($N > 5000$, mean = 0.15, standard deviation = 0.39). Wind field properties summarized over the annual cycle 2015 (see Figure S3) indicate a dominating SE (150°) wind directions and a mean wind speeds of 3.8 m $s^{-1}$. Analyzing the resulting set of $\xi$ in dependence of the wind conditions reveals distinct structures (Figure A2) that hint at an influence of the flow pattern on the self-heating

effect. The fraction $\xi$ is generally smallest within the SE sector (0.12 ± 0.28) followed by NE (0.13 ± 0.46), SW (0.16 ± 0.38), and highest values are observed in NW (0.22 ± 0.47). Under low wind speed conditions (e.g., around 300° in Figure A2) $\xi$ tends to be highest.

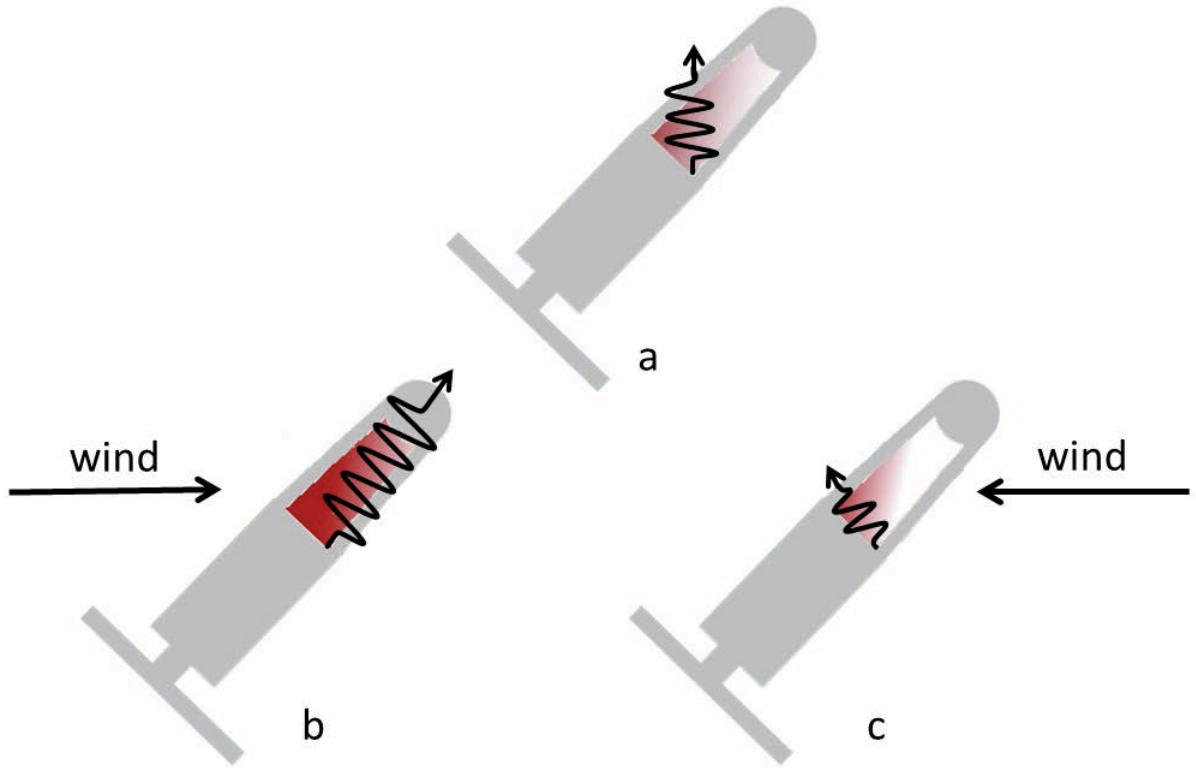


**Figure A1.** Conceptual overview of a potential wind direction impact on the self-heating effect for inclined OP sensors. (a) We separate calm conditions from conditions when the heated air is blown (b) into or (c) away from the measurement path. The red shaded area marks the volume within the measurement cell that is influenced by the heating, and the black curved arrow indicates the heat flux direction.

The OP sensor was installed in an inclined position by ~15° toward ESE (120°). Accordingly, with horizontal wind coming from the NW sector (240°–360°), air will be blown directly into the optical path, reinforcing the self-heating effect (Figure A1b). In contrast, the extra heat flux induced by the instrument self-heating will be transported out of the optical path with wind directions from the SE (60°–180°; Figure A1c). Focusing on the lower wind speeds (<4 m $s^{-1}$), this pattern can be observed in Figure A2: comparatively small $\xi$ are fitted for the E-SE sectors, indicating that the self-heating effect within these directions is smaller than average. In contrast, winds from the W-NW sectors can be associated with higher-than-average $\xi$, suggesting that heated air is directed into the optical path and leads to an amplified self-heating effect. For higher wind speeds (>4 m $s^{-1}$), we assume that the associated increase in mechanical turbulence generates a better mixing of the air around the sensors, therefore reducing the relative impact of the self-heating effect, and accordingly also the required $\xi$ to correct the fluxes. This can be seen in Figure A2 for almost all directions, except for the SW sector (190°–230°): For these directions, flow distortion by the sonic anemometer [*Göckede et al.*, 2008; *Mauder et al.*, 2007] under high wind speeds appears to influence the performance

of the OP sensor, leading to highly elevated $\xi$ that are unlikely to be caused by the instrument self-heating alone.

We found evidence that self-heating correction is influenced by flow patterns. Results presented here are used as a case study, since findings are not reproducible with the Burba_2008 approach. This indicates methodological uncertainties that need further investigations.

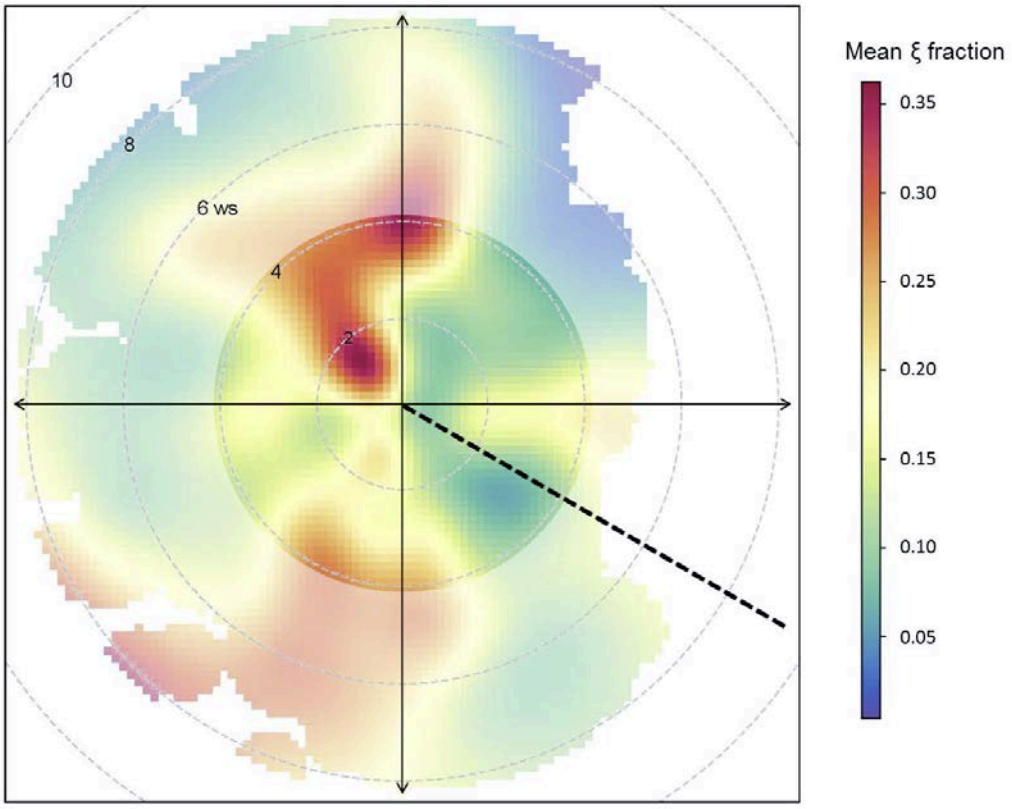


**Figure A2.** Averaged fraction $\xi$ (color coded) binned by wind direction ((°), black compass rose) and wind speed ((m $s^{-1}$), gray dashed circles). For the instrument surface temperature estimation equation 7 was used. The focus is set to small wind speeds up to 4 m $s^{-1}$ with semitransparent colors for higher wind speeds. The OP sensor is 15° toward ESE indicated by the black dashed line.

# Acknowledgments

This work was supported by the Max-Planck Society, the European Commission (PAGE21 project, FP7-ENV-2011, grant agreement 282700, and PerCCOM project, FP7-PEOPLE-2012-CIG, grant agreement PCIG12-GA-201-333796), the German Ministry of Education and Research (CarboPerm-Project, BMBF grant 03G0836G), the AXA Research Fund (PDOC_2012_W2 campaign, ARF fellowship M.Göckede), and the European Science Foundation (ESF for the activity “Tall tower and surface research network for verification of climate relevant emissions of human origin”, Short Visit Grant, fellowship F. Kittler). The authors appreciate the efforts of NESS staff members, especially Galina Zimova and Nastya Zimova, for organizing field work; they also recognize the team from the Field Experiments and Instrumentation group (MPI-BGC), especially Martin Hertel, for supporting field work.

We applied first-last-author-emphasis and equal-contribution (alphabetical sequence) methods for the order of authors [*Tscharntke et al*., 2007]. We thank one anonymous referee and Georg Burba for their valuable feedback and helpful comments and suggestions that strongly improved our manuscript. Data are available from the European Fluxes Database Cluster (http://www.europe-fluxdata.eu/home), site-code "RU-Ch2," with following options for the $CO_2$ flux: open-path gas data without the self-heating correction and open-path data with the self-heating correction and closed-path data.

# References

Amiro, B. (2010), Estimating annual carbon dioxide eddy fluxes using open-path analysers for cold forest sites, *Agric. For. Meteorol.*, 150(10), 1366–1372, doi:10.1016/j.agrformet.2010.06.007. A

Aubinet, M., L. Joly, D. Loustau, A. De Ligne, H. Chopin, J. Cousin, N. Chauvin, T. Decarpenterie, and P. Gross (2016), Dimensioning IRGA gas sampling systems: Laboratory and field experiments, *Atmos. Meas. Tech.*, 9(3), 1361–1367, doi:10.5194/amt-9-1361-2016.

Aubinet, M., T. Vesala, and D. Papale (2012), Eddy Covariance—A Practical Guide to Measurement and Data Analysis, p. 449, Springer, Dordrecht; Heidelberg; London; New York, doi:10.1029/2002JD002055.

Bate, G. C., and V. R. Smith (1983), Photosynthesis and respiration in the Sub-Antarctic Tussock Grass Poa-Cookii, *New Phytol.*, 95(4), 533–543, doi:10.1111/j.1469-8137.1983.tb03518.x.

Bowling, D. R., S. Bethers-Marchetti, C. K. Lunch, E. E. Grote, and J. Belnap (2010), Carbon, water, and energy fluxes in a semiarid cold desert grassland during and following multiyear drought, *J. Geophys. Res.*, 115, G04026, doi:10.1029/2010JG001322.

Burba, G. G., and D. J. Anderson (2010a), A Brief Practical Guide to Eddy Covariance Flux Measurements, p. 212, Li-COR Inc., Lincoln.

Burba, G. G., and D. J. Anderson (2010b), Part II. Eddy covariance workflow: Surface heat exchange and open-path gas fluxes from older analyzers, in A Brief Guide to Eddy Covariance Flux Measurements, Principles and Workflow Examples for Scientific and Industrial Applications, pp. 137–161, Li-COR Inc., Lincon.

Burba, G. G., D. J. Anderson, L. Xu, and D. K. McDermitt (2006), Correcting apparent off-season $CO_2$ uptake due to surface heating of a an open path gas analyzer: Process report of an ongoing study, in Proceedings of 27th Annual Conference on Agricultural and Forest Meteorology, p. 13, AMS, San Diego, Calif.

Burba, G. G., D. K. McDermitt, A. Grelle, D. J. Anderson, and L. Xu (2008), Addressing the influence of instrument surface heat exchange on the measurements of $CO_2$ flux from open-path gas analyzers, *Global Change Biol.*, 14(8), 1854–1876, doi:10.1111/j.1365-2486.2008.01606.x.

Carslaw, D. C. (2015), The openair manual—Open-source tools for analysing air pollution data, in Manual for Version 1.1–4, 287 pp., King's Collage, London.

Clement, R. J., G. G. Burba, A. Grelle, D. J. Anderson, and J. B. Moncrieff (2009), Improved trace gas flux estimation through IRGA sampling optimization, *Agric. For. Meteorol.*, 149(3–4), 623–638, doi:10.1016/j.agrformet.2008.10.008.

Coyne, P. I., and J. J. Kelley (1974), Carbon-dioxide partial pressures in Arctic surface waters, *Limnol. Oceanogr.*, 19(6), 928–938.

Dunn, G. (2004), Statistical Evaluation of Measurement Errors, p. 216, Arnold, London.

Eugster, W., and L. Merbold (2015), Eddy covariance for quantifying trace gas fluxes from soils, *Soil*, 1(1), 187–205, doi:10.5194/soil-1-187-2015.

Euskirchen, E. S., M. S. Bret-Harte, G. J. Scott, C. Edgar, and G. R. Shaver (2012), Seasonal patterns of carbon dioxide and water fluxes in three representative tundra ecosystems in northern Alaska, *Ecosphere*, 3(1), doi:10.1890/ES11-00202.1.

Foken, T. (2017), Micrometeorology, 2nd ed., p. 362, Springer, Berlin, doi:10.1007/978-3-642-25440-6.

Foken, T., M. Göockede, M. Mauder, L. Mahrt, B. Amiro, and W. Munger (2005), Post-field data quality control, in Handbook of Micrometeorology: A Guide for Surface Flux Measurement and Analysis, edited by X. Lee, W. Massman and B. Law, pp. 181–208, Springer, Dordrecht, Netherlands, doi:10.1007/1-4020-2265-4_9.

Foken, T., R. Leuning, S. P. Oncley, M. Mauder, and M. Aubinet (2012), Corrections and data quality, in Eddy Covariance—A Practical Guide to Measurement and Data Analysis, edited by M. Aubinet, T. Vesala, and D. Papale, pp. 85–131, Springer, Dordrecht, Netherlands.

Foken, T., and B. Wichura (1996), Tools for quality assessment of surface-based flux measurements, *Agric. For. Meteorol.*, 78(1–2), 83–105, doi:10.1016/0168-1923(95)02248-1.

Fratini, G., and M. Mauder (2014), Towards a consistent eddy-covariance processing: An intercomparison of EddyPro and TK3, *Atmos. Meas. Tech.*, 7(7), 2273–2281, doi:10.5194/amt-7-2273-2014.

Göckede, M., et al. (2008), Quality control of CarboEurope flux data—Part 1: Coupling footprint analyses with flux data quality assessment to evaluate sites in forest ecosystems, *Biogeosciences*, 5(2), 433–450, doi:10.5194/bg-5-433-2008.

Goodrich, J. P., W. C. Oechel, B. Gioli, V. Moreaux, P. C. Murphy, G. Burba, and D. Zona (2016), Impact of different eddy covariance sensors, site set-up, and maintenance on the annual balance of CO2 and CH4 in the harsh Arctic environment, *Agric. For. Meteorol.*, 228–229, 239–251, doi:10.1016/j.agrformet.2016.07.008.

Grelle, A., and G. Burba (2007), Fine-wire thermometer to correct $CO_2$ fluxes by open-path analyzers for artificial density fluctuations, *Agric. For. Meteorol.*, 147(1–2), 48–57, doi:10.1016/j.agrformet.2007.06.007.

Grogan, P., A. Michelsen, P. Ambus, and S. Jonasson (2004), Freeze-thaw regime effects on carbon and nitrogen dynamics in sub-arctic heath tundra mesocosms, *Soil Biol. Biochem.*, 36(4), 641–654, doi:10.1016/j.soilbio.2003.12.007.

Haslwanter, A., A. Hammerle, and G. Wohlfahrt (2009), Open-path vs. closed-path eddy covariance measurements of the net ecosystem carbon dioxide and water vapour exchange: A long-term perspective, *Agric. For. Meteorol.*, 149(2), 291–302, doi:10.1016/j.agrformet.2008.08.011.

Helbig, M., et al. (2016), Addressing a systematic bias in carbon dioxide flux measurements with the EC150 and the IRGASON open-path gas analyzers, *Agric. For. Meteorol.*, 228, 349–359, doi:10.1016/j.agrformet.2016.07.018.

Järvi, L., I. Mammarella, W. Eugster, A. Ibrom, E. Siivola, E. Dellwik, P. Keronen, G. Burba, and T. Vesala (2009), Comparison of net $CO_2$ fluxes measured with open- and closed-path infrared gas analyzers in an urban complex environment, *Boreal Environ. Res.*, 14(4), 499–514.

Kappen, L. (1993), Plant activity under snow and ice, with particular reference to lichens, *Arctic*, 46(4), 297–302.

Kelley, J. J., D. F. Weaver, and B. P. Smith (1968), Variation of carbon dioxide under snow in Arctic, *Ecology*, 49(2), 358–361, doi:10.2307/1934472.

Kittler, F., I. Burjack, C. A. R. Corradi, M. Heimann, O. Kolle, L. Merbold, N. Zimov, S. Zimov, and M. Göckede (2016), Impacts of a decadal drainage disturbance on surface–atmosphere fluxes of carbon dioxide in a permafrost ecosystem, *Biogeosciences*, 13(18), 5315–5332, doi:10.5194/bg-13-5315-2016.

Kolle, O., and C. Rebmann (2007), EddySoft; documentation of a software package to acquire and process Eddy covariance data, Rep., Jena.

Legendre, P. (Ed.) (2014), lmodel2: Model II Regression.

Leuning, R. (2004), Measurements of trace gas fluxes in the atmosphere using eddy covariance: WPL corrections revisited, in Handbook of Micrometeorology: A Guide for Surface Flux Measurements and Analysis, edited by X. Lee, W. Massman, and B. Law, pp. 119–132, Kluwer Acad., Dordrecht, Netherlands.

Leuning, R. (2007), The correct form of the Webb, Pearman and Leuning equation for eddy fluxes of trace gases in steady and non-steady state, horizontally homogeneous flows, *Boundary-Layer Meteorol.*, 123(2), 263–267, doi:10.1007/s10546-006-9138-5.

Liu, H. P., G. Peters, and T. Foken (2001), New equations for sonic temperature variance and buoyancy heat flux with an omnidirectional sonic anemometer, *Boundary Layer Meteorol.*, 100(3), 459–468, doi:10.1023/A:1019207031397.

Lüers, J., S. Westermann, K. Piel, and J. Boike (2014), Annual $CO_2$ budget and seasonal $CO_2$ exchange signals at a high Arctic permafrost site on Spitsbergen, Svalbard archipelago, *Biogeosciences*, 11(22), 6307–6322, doi:10.5194/bg-11-6307-2014.

Makkonen, L., and T. Laakso (2005), Humidity measurements in cold and humid environments, *Boundary Layer Meteorol.*, 116(1), 131–147, doi:10.1007/s10546-004-7955-y.

Marushchak, M. E., I. Kiepe, C. Biasi, V. Elsakov, T. Friborg, T. Johansson, H. Soegaard, T. Virtanen, and P. J. Martikainen (2013), Carbon dioxide balance of subarctic tundra from plot to regional scales, *Biogeosciences*, 10(1), 437–452, doi:10.5194/bg-10-437-2013.

Massman, W., and J. Frank (2009), Three issues concerning open- and closed-path sensors: Self-heating, pressure effects, and tube wall adsorption, in AsiaFlux Workshop, 167 pp., Sapporo, Japan.

Mastepanov, M., C. Sigsgaard, E. J. Dlugokencky, S. Houweling, L. Strom, M. P. Tamstorf, and T. R. Christensen (2008), Large tundra methane burst during onset of freezing, *Nature*, 456(7222), 628–630, doi:10.1038/nature07464.

Mauder, M., and T. Foken (2015), Eddy-covariance software TK3, doi:10.5281/zenodo.20349.

Mauder, M., S. P. Oncley, R. Vogt, T. Weidinger, L. Ribeiro, C. Bernhofer, T. Foken, W. Kohsiek, H. A. R. De Bruin, and H. Liu (2007), The energy balance experiment EBEX-2000. Part II: Intercomparison of eddy-covariance sensors and post-field data processing methods, *Boundary Layer Meteorol.*, 123(1), 29–54, doi:10.1007/s10546-006-9139-4.

Metzger, S., G. Burba, S. P. Burns, P. D. Blanken, J. H. Li, H. Y. Luo, and R. C. Zulueta (2016), Optimization of an enclosed gas analyzer sampling system for measuring eddy covariance fluxes of $H_2O$ and $CO_2$, *Atmos. Meas. Tech.*, 9(3), 1341–1359, doi:10.5194/amt-9-1341-2016.

Monson, R., and D. Baldocchi (2014) Terrestrial Biosphere-Atmosphere Fluxes, p. 487, Cambridge Univ. Press, Cambridge.

Moore, C. J. (1986), Frequency response corrections for eddy correlation systems, *Boundary Layer Meteorol.*, 37(1–2), 17–35, doi:10.1007/Bf00122754.

Munger, J. W., H. W. Loescher, and H. Luo (2012), Measurement, tower, and site design considerations, in Eddy Covariance—A Practical Guide to Measurement and Data Analysis, edited by M. Aubinet, T. Vesala, and D. Papale, pp. 21–58, Springer, Dordrecht, Netherlands.

Nobel, P. S. (1983), Biophysical Plant Physiology, W. H. Freeman, San Francisco, Calif.

Oechel, W. C., C. A. Laskowski, G. Burba, B. Gioli, and A. A. M. Kalhori (2014), Annual patterns and budget of $CO_2$ flux in an Arctic tussock tundra ecosystem, *J. Geophys. Res. Biogeosci.*, 119, 323–339, doi:10.1002/2013jg002431.

Oechel, W. C., G. Vourlitis, and S. J. Hastings (1997), Cold season $CO_2$ emission from Arctic soils, *Global Biogeochem. Cycles*, 11, 163–172, doi:10.1029/96gb03035.

Ono, K., A. Miyata, and T. Yamada (2007), Apparent downward $CO_2$ flux observed with open-path eddy covariance over a non-vegetated surface, *Theor. Appl. Climatol.*, 92(3–4), 195–208, doi:10.1007/s00704-007-0323-3.

Panikov, N. S., P. W. Flanagan, W. C. Oechel, M. A. Mastepanov, and T. R. Christensen (2006), Microbial activity in soils frozen to below −39 degrees C, *Soil Biol. Biochem.*, 38(4), 785–794, doi:10.1016/j.soilbio.2006.06.004.

Pries, C. E. H., E. A. G. Schuur, and K. G. Crummer (2013), Thawing permafrost increases old soil and autotrophic respiration in tundra: Partitioning ecosystem respiration using delta C-13 and Delta C-14, *Global Change Biol.*, 19(2), 649–661, doi:10.1111/gcb.12058.

Core Team, R. (2014), R: A Language and Environment for Statistical Computing, R Foundation for Statistical Computing, Vienna, Austria.

Reichstein, M., et al. (2005), On the separation of net ecosystem exchange into assimilation and ecosystem respiration: Review and improved algorithm, *Global Change Biol.*, 11(9), 1424–1439, doi:10.1111/j.1365-2486.2005.001002.x.

Reverter, B. R., et al. (2011), Adjustment of annual NEE and ET for the open-path IRGA self-heating correction: Magnitude and approximation over a range of climate, *Agric. For. Meteorol.*, 151(12), 1856–1861, doi:10.1016/j.agrformet.2011.06.001.

Rogiers, N., F. Conen, M. Furger, R. Stockli, and W. Eugster (2008), Impact of past and present land-management on the C-balance of a grassland in the Swiss Alps, *Global Change Biol.*, 14(11), 2613–2625, doi:10.1111/j.1365-2486.2008.01680.x.

Skelly, B. T., D. R. Miller, and T. H. Meyer (2002), Triple-hot-film anemometer performance in Cases-99 and a comparison with sonic anemometer measurements, *Boundary Layer Meteorol.*, 105(2), 275–304, doi:10.1023/A:1019906521898.

Stull, R. B. (1988), An Introduction to Boundary Layer Meteorology, p. 666, Kluwer Acad., Dordrecht, Netherlands.

Tscharntke, T., M. E. Hochberg, T. A. Rand, V. H. Resh, and J. Krauss (2007), Author sequence and credit for contributions in multiauthored publications, *PLoS Biol.*, 5(1), 13–14, doi:10.1371/journal.pbio.0050018.

Ueyama, M., R. Hirata, M. Mano, K. Hamotani, Y. Harazono, T. Hirano, A. Miyata, K. Takagi, and Y. Takahashi (2012), Influences of various calculation options on heat, water and carbon fluxes determined by open- and closed-path eddy covariance methods, *Tellus, Ser. B: Chem. Phys. Meteorol.*, 64, doi:10.3402/tellusb.v64i0.19048.

Webb, E. K., G. I. Pearman, and R. Leuning (1980), Correction of flux measurements for density effects due to heat and water vapour transfer, *Q. J. R. Meteorol. Soc.*, 106(447), 85–100, doi:10.1002/qj.49710644707.

Wohlfahrt, G., L. F. Fenstermaker, and J. A. Arnone (2008), Large annual net ecosystem CO2 uptake of a Mojave Desert ecosystem, *Global Change Biol.*, 14(7), 1475–1487, doi:10.1111/j.1365-2486.2008.01593.x.

Wyngaard, J. C. (2010), Turbulence in the Atmosphere, p. 406, Cambridge Univ. Press, Cambridge.

Zimov, S. A., S. P. Davidov, Y. V. Voropaev, I. P. Semiletov, M. C. Chapin, and F. S. Chapin III (1996), Siberian $CO_2$ efflux in winter as a $CO_2$ source and cause of seasonality in atmospheric $CO_2$, *Clim. Change*, 33(1), 111–120, doi:10.1007/Bf00140516.

Zimov, S. A., S. P. Daviodov, Y. V. Voropaev, and S. F. Prosiannikov (1993), Planetary maximum $CO_2$ and ecosystems of the north, paper presented at Carbon Cycling in Boreal Forest and Sub-arctic Ecosystems: Biospheric Responses and Feedbacks to Global Climate Change, Department of Civil Engineering, Oregon State Univ., Corvallis, Oregon.

Zona, D., et al. (2016), Cold season emissions dominate the Arctic tundra methane budget, *Proc. Natl. Acad. Sci. U.S.A.*, 113(1), 40–45, doi:10.1073/pnas.1516017113.